Physics – Uspekhi **48** (9) 917 – 937 (2005)

INSTRUMENTS AND METHODS OF INVESTIGATION PACS numbers: **07.50. – e**, **41.75. – i**, **84.40. – x**, 84.40.Fe

Transverse electron-beam waves for microwave electronics

V A Vanke

DOI: 10.1070/PU2005v048n09ABEH002397

Contents

Abstract. A brief discussion is given of the state of the art, challenges, and prospects in the application of transverse (cyclotron and synchronous) electron-beam waves in microwave electronic devices, including protectors, parametric and electrostatic amplifiers, tunable filters, circularly polarized traveling wave tubes, microwave/DC converters, and combined interaction klystrons.

1. Introduction

The advent of electron tubes in the 1920s was a remarkable breakthrough that provided the impetus for the establishment of radiophysics as a science and greatly enlarged the possibilities for the application of electromagnetic oscillations and waves for the solution of many applied tasks. These tasks required the use of new, increasingly shorter wavelength ranges, first and foremost for the rapidly developing radar technology during the Second World War. Progress was slowed by transit effects in classical electron tubes. So-called lighthouse tubes were proposed as an engineering solution to minimize transit angles. This, however, failed to effectively overcome the problem.

The first attempt to take advantage of transit effects appears to have been made in the monotron [1, 2], the simplest diode generator in which electron inertia was a positive phenomenon leading to the formation of a volt – amper characteristic segment with negative internal resistance.

A qualitatively new step was the understanding of the principles of dynamic electron beam control that were used to develop a new class of electronic devices, viz. klystrons, traveling wave tubes (TWTs), backward wave tubes (BWTs), etc. [1 – 9]. These devices made it possible to fairly satisfactorily generate and amplify microwave oscillations, i.e., oscillations in the decimeter, centimeter, and millimeter wavelength ranges. Later on, cross-field generators and amplifiers were proposed (the magnetron, amplitron, TWT-M, BWT-M, etc.) [2, 4, 5, 7 – 9]. The application of the phase grouping principle to long-term interactions of weakly relativistic beams with electromagnetic fields [10] was employed to develop new powerful millimeter-wavelength amplifiers and generators or cyclotron-resonance masers (gyrotrons).

Microwave radiophysics and electronics had quite different objectives at different stages of their development. At an early stage, it was most important to have the possibility to generate strong oscillations and receive weak signals. Accordingly, the main parameters for which improvements were sought at that time were the output power for emitting systems and the amplification coefficient for receiving ones. Later on, it proved necessary to further increase the efficiency of powerful generators and amplifiers; this drew attention to the analysis and optimization of nonlinear regimes and the development of relevant models and ideas [11 – 14].

The majority of modern microwave systems make use of the cascade or multistage amplification and generate a complex modulated signal. This poses a controversial problem of how to achieve high efficiency at a large output power without the loss of information contained in the signal being amplified.

In this context, a receiving system depends not only on the amplification and noise factors but also on the degree of

V A Vanke Lomonosov Moscow State University,
Vorob'evy gory, 119992 Moscow, Russian Federation
Tel. (7-095) 132 48 07
E-mail: vanke@orc.ru

Received 23 December 2004, revised 19 May 2005
Uspekhi Fizicheskikh Nauk **175** (9) 957 – 978 (2005)
Translated by Yu V Morozov; edited by A M Semikhatov

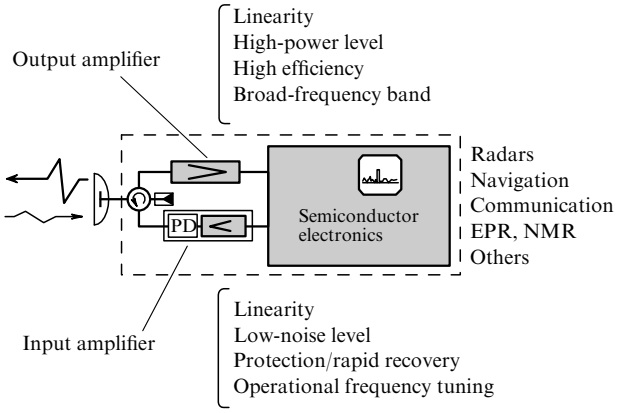

Figure 1. Schematic representation of microwave systems: PD — protective device preventing the fall of powerful pulses into the input of a low-noise amplifier.

linearity and noise resistance of the input amplifier, dynamic range width, filtration efficiency, large electric strength, rapid recovery after high overloads by input signals, etc. These characteristics acquire critical importance in light of frequency channel compression in the microwavelength range and intense development of radio-jamming technologies. They are sought even to the detriment of such parameters as the size, weight, and cost of a respective device, its amplification coefficient, and sometimes its noise factor.

Figure 1 presents a simplified scheme of the most widely used microwave systems and illustrates the principal requirements for their input and output amplifying cascades.

Solid state (semiconductor) microwave electronics has been rapidly developing during the last decades and has brought about a number of big achievements. However, vacuum electronics turns out to be the choice technology for the construction of cascading microwave devices in which high levels of continuous or pulsed microwave power are present or may be present.

Previously, microwave radiophysics was largely concerned with the use of electromagnetic beams in a variety of information transmission systems. In the last decades, however, it has focused on a more complicated and challenging task of applying these beams in energy transfer systems. Prospects of extraterrestrial industrial developments including production of energy to be consumed on the Earth [15–18] place microwave radiophysics at the forefront of modern science and technology. This accounts for the importance of the construction of both powerful microwave amplifiers and high-efficiency generators to be used in space-based antenna arrays and reliable energy-consuming devices for efficacious back conversion of microwave energy into direct current.

The use of the traditional longitudinal grouping of electrons into bunches in vacuum microwave electronics (e.g., in klystrons, TWTs, etc.) encounters serious problems arising from the nonlinear character of Coulomb forces that usually play an important role in the formation of electron bunches and in the energy exchange between them and external electromagnetic fields.

In many cases, these problems can be overcome (or eliminated) by the transverse grouping of the uniformly charged electron beam drifting in a longitudinal magnetic field (Fig. 2).

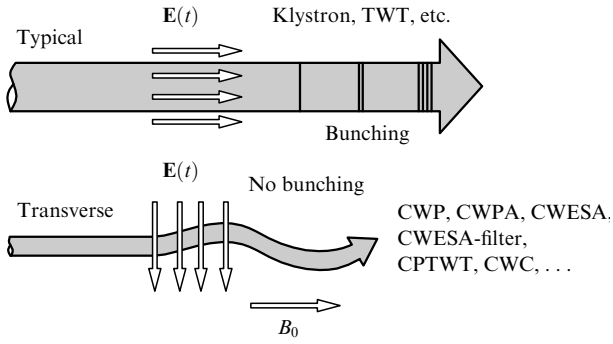

Figure 2. Longitudinal and transverse grouping of an electron beam: $\mathbf{E}(t)$ — time-variable electric field, B_0 — constant magnetic field.

The present review considers prospects for the application of the transverse grouping in various microwave devices and thus supplements previous publications in *Physics – Uspekhi* on the problems of vacuum microwave electronics [14, 19, 20] and extends their subject matter.

The set of devices based on the use of transverse electron-beam waves has been substantially enlarged during the last few decades to include, among others, industrially manufactured cyclotron-wave protectors. A better understanding of the physical principles underlying cyclotron wave amplification by electrostatic structures has led to the creation of centimeter-wavelength devices. Likewise, the principles of the operation of narrow-band electrically tunable input amplifier filters were formulated and tested in experiment. Many experimental data obtained with the use of circularly polarized traveling wave tubes (CPTWTs), a new type of powerful amplifier, were explained; also, the theory of CPTWTs was developed. A number of theoretical and experimental studies were carried out with a view to developing powerful devices for efficacious back conversion of microwave energy into direct current energy. Combined (longitudinal – transverse) interactions were shown to be of value for some specific purposes.

The most extensive investigations in these fields were conducted at Lomonosov Moscow State University, the 'Istok' and 'Tory' State Research and Production Corporations, and some other settings.

Rather a wide range of promising gyrotron-type devices (Institute of Applied Physics, Russian Academy of Sciences) and magnicons (Institute of Nuclear Physics, Siberian Branch of the Russian Academy of Sciences) using relativistic electron beams remain beyond the scope of this paper and might be the subject of a separate interesting review.

2. Some approaches to the analysis of transverse electron-beam oscillations and waves

2.1 Kinematic analysis

We consider electron motions in crossed electric and magnetic fields

$$\mathbf{E} = (E_x, E_y, 0)\,, \quad \mathbf{B} = (0, 0, B_0)\,, \quad B_0 = \text{const}\,. \tag{1}$$

The introduction of the complex transverse coordinate $\zeta(t) = x(t) + \mathrm{i}y(t)$ of the electron by the simple and efficient method of P L Kapitsa [8] allows the nonrelativistic equation

of motion to be written as:

$$\frac{\mathrm{d}^2\zeta}{\mathrm{d}t^2} - \mathrm{i}\omega_\mathrm{c}\,\frac{\mathrm{d}\zeta}{\mathrm{d}t} = f, \quad v_z = \mathrm{const}\,, \tag{2}$$

where $f = -e(E_x + \mathrm{i}E_y)/m$, $\omega_\mathrm{c} = (e/m)\,B_0$ is the angular dependence, and v_z, e, and m are the electron longitudinal velocity, charge, and mass, respectively.

In the unperturbed case ($f = 0$), the solution of Eqn (2) has the form

$$\zeta = \alpha + \beta\exp(\mathrm{i}\omega_\mathrm{c}t)\,, \tag{3}$$

where α, β are constants; in other words, the electron can move in a spiral path rotating with the angular frequency ω_c and radius $|\beta|$ around an axis parallel to the z axis and shifted by the distance $|\alpha|$ with respect to it.

In case of perturbation $f \neq 0$, the solution should be sought in the form

$$\zeta(t) = \alpha(t) + \beta(t)\exp(\mathrm{i}\omega_\mathrm{c}t)\,. \tag{4}$$

Because (4) contains two new variables instead of one, it is possible to use an additional condition

$$\frac{\mathrm{d}\alpha}{\mathrm{d}t} + \frac{\mathrm{d}\beta}{\mathrm{d}t}\exp(\mathrm{i}\omega_\mathrm{c}t) = 0\,. \tag{4a}$$

Two first-order differential equations for α and β that describe changes in these quantities under the effect of the external electric field then follow from Eqn (2):

$$\begin{aligned}\frac{\mathrm{d}\alpha}{\mathrm{d}t} &= \frac{\mathrm{i}}{\omega_\mathrm{c}}\,f(\alpha,\alpha^*,\beta,\beta^*,t)\,,\\ \frac{\mathrm{d}\beta}{\mathrm{d}t} &= -\frac{\mathrm{i}}{\omega_\mathrm{c}}\,f(\alpha,\alpha^*,\beta,\beta^*,t)\,\exp(-\mathrm{i}\omega_\mathrm{c}t)\,.\end{aligned} \tag{5}$$

In the adiabatic case, when the intensity of the electric field is rather low and causes small relative changes to α and β during the cyclotron rotation period, it is possible to average the right-hand sides of Eqns (5) over the period $2\pi/\omega_\mathrm{c}$, a procedure well known from the theory of oscillations, i.e.,

$$\begin{aligned}\frac{\mathrm{d}\alpha}{\mathrm{d}t} &= \frac{\mathrm{i}}{2\pi\omega_\mathrm{c}}\int_0^{2\pi} f(\alpha,\alpha^*,\beta,\beta^*,t)\,\mathrm{d}(\omega_\mathrm{c}t)\,,\\ \frac{\mathrm{d}\beta}{\mathrm{d}t} &= -\frac{\mathrm{i}}{2\pi\omega_\mathrm{c}}\int_0^{2\pi} f(\alpha,\alpha^*,\beta,\beta^*,t)\,\exp(-\mathrm{i}\omega_\mathrm{c}t)\,\mathrm{d}(\omega_\mathrm{c}t)\,.\end{aligned} \tag{6}$$

The asymptotic methods of the nonlinear oscillation theory [21] allow the construction of the second approximation [16, 22, 23] taking into consideration, in particular, small vibrations supplementing the principal solution of the system (signal and pump harmonics, higher combination frequencies, etc.).

2.2 Transverse electron-beam waves

The notion of transverse electron-beam waves has been in use for a rather long time [12, 19–27] but is strictly speaking substantiated only for the model of filamentary electron beams.

We consider the longitudinal coordinate z and time t in Eqn (2) to be independent variables, i.e.,

$$\zeta(z,t) = x(z,t) + \mathrm{i}y(z,t)\,, \tag{7}$$

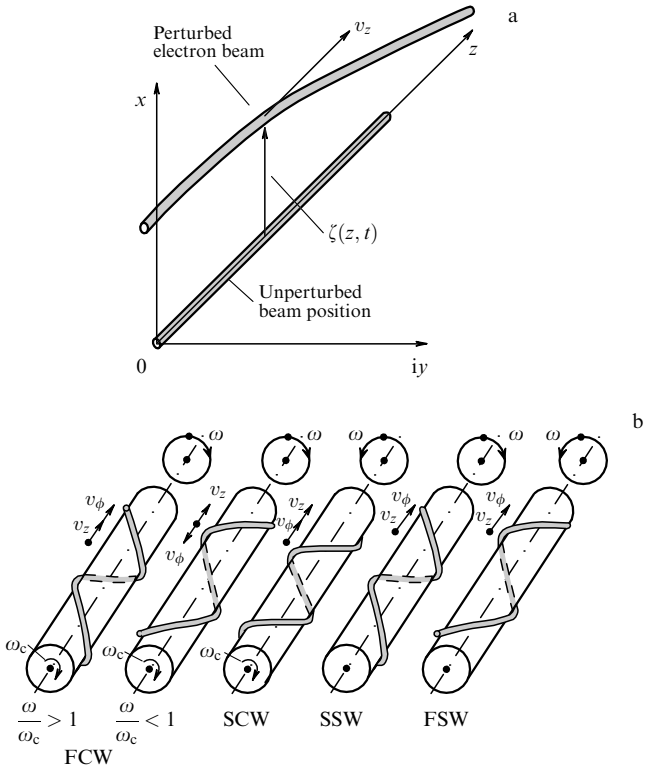

Figure 3. (a) Model of a filamentary electron beam. (b) Spatial configuration of a filamentary electron beam excited at different transverse waves: FCW — fast cyclotron wave, SCW — slow cyclotron wave, SSW, FSW — synchronous waves with different polarization (the internal cylinder serves only for illustrative purposes).

thus passing from the description of motion of an individual electron to the description of the behavior of a filamentary electron beam (Fig. 3a).

We search for the solution in the form of the sum of two right and left circularly polarized waves,

$$\begin{aligned}\zeta(z,t) = {} & R_+(z)\,\exp\left[\mathrm{i}(\omega t - \beta_\mathrm{e}z)\right]\\ & + R_-(z)\exp\left[-\mathrm{i}(\omega t - \beta_\mathrm{e}z)\right],\end{aligned} \tag{8}$$

where $\beta_\mathrm{e} = \omega/v_z$ is the electron propagation constant and the functions $R_\pm$ depend on the longitudinal coordinate z alone.

Substituting Eqn (8) in (2) and representing f as

$$f = f_+\exp\left[\mathrm{i}(\omega t - \beta_\mathrm{e}z)\right] + f_-\exp\left[-\mathrm{i}(\omega t - \beta_\mathrm{e}z)\right], \tag{9}$$

and also taking into consideration that

$$\frac{\mathrm{d}}{\mathrm{d}t} = \frac{\partial}{\partial t} + v_z\,\frac{\partial}{\partial z} \quad \mathrm{i} \quad \frac{\partial}{\partial z}\,R_\pm = \frac{\mathrm{d}}{\mathrm{d}z}\,R_\pm\,, \tag{10}$$

leads to

$$\frac{\mathrm{d}^2R_\pm}{\mathrm{d}z^2} - \mathrm{i}\beta_\mathrm{c}\,\frac{\mathrm{d}R_\pm}{\mathrm{d}z} = \frac{1}{v_z^2}\,f_\pm\,, \tag{11}$$

where $\beta_\mathrm{c} = \omega_\mathrm{c}/v_z$ is the cyclotron propagation constant.

In the drift region ($f_\pm = 0$),

$$R_\pm = R_{2\pm} + R_{1\pm}\exp(\mathrm{i}\beta_\mathrm{c}z)\,, \tag{12}$$

where $R_{2\pm}$, $R_{1\pm}$ are certain constants and, accordingly,

$$\begin{aligned}\zeta(z,t) = {} & R_{1+}\exp\left\{\mathrm{i}\left[\omega t-(\beta_\mathrm{e}-\beta_\mathrm{c})\,z\right]\right\}\\ & + R_{2+}\exp\left[\mathrm{i}\,(\omega t-\beta_\mathrm{e}z)\right]\\ & + R_{1-}\exp\left\{-\mathrm{i}\left[\omega t-(\beta_\mathrm{e}+\beta_\mathrm{c})\,z\right]\right\}\\ & + R_{2-}\exp\left[-\mathrm{i}(\omega t-\beta_\mathrm{e}z)\right].\end{aligned} \tag{13}$$

Thus, the configuration of a filamentary electron beam drifting in a uniform magnetic field may be described by four independent waves, two of which (with amplitudes $R_{1\pm}$) are related to cyclotron rotation of electrons and termed cyclotron. Two others (with amplitudes $R_{2\pm}$) have the phase velocities equal to the beam longitudinal velocity; they are usually called synchronous waves. One pair of waves (with the subscripts $1+$ and $2+$) has right circular polarization, the other (with the subscripts $1-$ and $2-$) is left-circularly polarized.

The respective phase velocities of transverse waves are

$$v_{\phi 1\pm}=\frac{v_z}{1\mp\omega_\mathrm{c}/\omega}\,,\quad v_{\phi 2\pm}=v_z\,. \tag{14}$$

The phase velocity of a cyclotron wave with a complex amplitude R_{1+} may be significantly higher than the longitudinal velocity of the electron beam. For this reason, this wave is called a fast cyclotron wave (FCW). The phase velocity of a wave with the amplitude R_{1-} is always lower than the beam longitudinal velocity, hence its name, slow cyclotron wave (SCW). Electrons of a beam excited on cyclotron waves are involved in two types of motion: rotation about the z axis at the angular frequency ω_c and propagation along the z axis with the velocity v_z (Fig. 3b). In all cases, at a fixed moment of time, the electrons are spatially shifted with respect to one another, thereby forming a spiral. For a fast cyclotron wave, the spirals at $\omega/\omega_\mathrm{c}>1$ and $\omega/\omega_\mathrm{c}<1$ have opposite winding. At the cyclotron resonance point ($\omega/\omega_\mathrm{c}=1$), the phase velocity of FCW tends to infinity, and all beam electrons happen to lie on a straight line rotating as a whole around the z axis at the angular frequency $\omega_\mathrm{c}=\omega$ and moving along the z axis with the velocity v_z. Beam configurations for synchronous waves (with the amplitudes R_{2+} and R_{2-}) are different in terms of winding direction in spirals, but all electrons of these spirals are lacking transverse velocities and participate in only a single type of motion, along the z axis.

We now consider the case where a static magnetic field and the longitudinal velocity of electrons may change along the z axis. Instead of (2), we then have the expression

$$\frac{\mathrm{d}^2\zeta}{\mathrm{d}t^2}-\mathrm{i}\omega_{\mathrm{c}0}(z)\,\frac{\mathrm{d}\zeta}{\mathrm{d}t}=F(\zeta,\zeta^*,z,t)\,,\quad v_z=v_z(z)\,, \tag{15}$$

where $\omega_{\mathrm{c}0}(z)=\omega_\mathrm{c}(z,x=0,y=0)$ is the value of the cyclotron frequency at the z axis. We further write

$$F=F_+\exp\left[\mathrm{i}\left(\omega t-\int_0^z\beta_\mathrm{e}\,\mathrm{d}z\right)\right]+F_-\exp\left[-\mathrm{i}\left(\omega t-\int_0^z\beta_\mathrm{e}\,\mathrm{d}z\right)\right], \tag{16}$$

$$\begin{aligned}\zeta(z,t) = {} & R_+(z)\exp\left[\mathrm{i}\left(\omega t-\int_0^z\beta_\mathrm{e}\,\mathrm{d}z\right)\right]\\ & + R_-(z)\exp\left[-\mathrm{i}\left(\omega t-\int_0^z\beta_\mathrm{e}\,\mathrm{d}z\right)\right],\end{aligned} \tag{17}$$

where $\beta_\mathrm{e}(z)=\omega/v_z(z)$.

Relations (15)–(17) yield

$$\begin{aligned}&\frac{\mathrm{d}^2R_\pm}{\mathrm{d}\Theta^2}-\mathrm{i}\,\frac{\mathrm{d}R_\pm}{\mathrm{d}\Theta}=\frac{1}{\omega_{\mathrm{c}0}^2}\,F_\pm-\frac{1}{\omega_{\mathrm{c}0}}\,\frac{\mathrm{d}\omega_{\mathrm{c}0}}{\mathrm{d}\Theta}\,\frac{\mathrm{d}R_\pm}{\mathrm{d}\Theta}\,,\\ &\Theta=\int_0^z\omega_{\mathrm{c}0}(z)\,\frac{\mathrm{d}z}{v_z(z)}\end{aligned} \tag{18}$$

instead of (11). In the method of variation of constants, the solution is sought in the form

$$R_\pm(\Theta)=R_{2\pm}(\Theta)+R_{1\pm}(\Theta)\,\exp(\mathrm{i}\Theta)\,, \tag{19}$$

i.e.,

$$\begin{aligned}\zeta(z,t) = {} & R_{1+}(\Theta)\,\exp\left\{\mathrm{i}\left[\omega t-\int_0^z(\beta_\mathrm{e}-\beta_\mathrm{c})\,\mathrm{d}z\right]\right\}\\ & + R_{2+}(\Theta)\,\exp\left[\mathrm{i}\left(\omega t-\int_0^z\beta_\mathrm{e}\,\mathrm{d}z\right)\right]\\ & + R_{1-}(\Theta)\exp\left\{-\mathrm{i}\left[\omega t-\int_0^z(\beta_\mathrm{e}+\beta_\mathrm{c})\,\mathrm{d}z\right]\right\}\\ & + R_{2-}(\Theta)\,\exp\left[-\mathrm{i}\left(\omega t-\int_0^z\beta_\mathrm{e}\,\mathrm{d}z\right)\right].\end{aligned} \tag{20}$$

Substituting (19) into (18) and using additional conditions similar to (4a),

$$\frac{\mathrm{d}R_{2\pm}(\Theta)}{\mathrm{d}\Theta}+\frac{\mathrm{d}R_{1\pm}(\Theta)}{\mathrm{d}\Theta}\exp(\mathrm{i}\Theta)=0\,, \tag{21}$$

leads to four first-order differential equations describing the behavior of transverse wave amplitudes:

$$\begin{aligned}\frac{\mathrm{d}R_{1\pm}}{\mathrm{d}\Theta} = {} & -\frac{\mathrm{i}}{\omega_{\mathrm{c}0}^2}\,F_\pm(R_{1\pm},R_{2\pm},R_{1\pm}^*,R_{2\pm}^*,\Theta)\\ & \times\exp(-\mathrm{i}\Theta)-\frac{1}{\omega_{\mathrm{c}0}}\,\frac{\mathrm{d}\omega_{\mathrm{c}0}}{\mathrm{d}\Theta}\,R_{1\pm}\,,\\ \frac{\mathrm{d}R_{2\pm}}{\mathrm{d}\Theta} = {} & \frac{\mathrm{i}}{\omega_{\mathrm{c}0}^2}\,F_\pm(R_{1\pm},R_{2\pm},R_{1\pm}^*,R_{2\pm}^*,\Theta)\\ & +\frac{1}{\omega_{\mathrm{c}0}}\,\frac{\mathrm{d}\omega_{\mathrm{c}0}}{\mathrm{d}\Theta}\,R_{1\pm}\exp(\mathrm{i}\Theta)\,.\end{aligned} \tag{22}$$

In the adiabatic case, as for Eqns (5), system of equations (22) may be treated by averaging their right-hand sides over the fast oscillation period; asymptotic methods of the nonlinear oscillation theory [21] for the construction of the above first-order approximations are also applicable.

In the case of short electric and magnetic lenses, when the transit angle inside the interaction region changes insignificantly, the right-hand sides of Eqns (22) may be considered to contain $\exp(\pm\mathrm{i}\Theta)\approx 1$; this is usually conducive to the substantial simplification of the analytic solution of the problem.

2.3 Kinetic powers of transverse waves

The period-averaged power of energy exchange between transverse waves and electromagnetic fields has been computed as the sum of powers of energy exchanges with longitudinal and transverse components of the electric

field [1]

$$P_{1\pm} = P_{1\pm}^{\text{trans}} + P_{1\pm}^{\text{long}} = \pm I_0 U_0 \beta_e \beta_{c0} |R_{1\pm}|^2 , \tag{23}$$

with

$$P_{1\pm}^{\text{trans}} = \frac{I_0}{e}\,\frac{m v_\perp^2}{2} = \frac{I_0}{e}\,\frac{m\left(\omega_{c0}|R_{1\pm}|\right)^2}{2} ,$$
$$P_{1\pm}^{\text{long}} = \pm \frac{I_0 m}{2e}\,\omega_{c0}(\omega \mp \omega_{c0})|R_{1\pm}|^2 , \tag{24}$$

$$P_{2\pm} = P_{2\pm}^{\text{long}} = \mp I_0 U_0 \beta_e \beta_{c0} |R_{2\pm}|^2 , \quad P_{2\pm}^{\text{trans}} = 0 , \tag{25}$$

where I_0 and U_0 are the current and the potential of the electron beam, respectively.

There is no energy exchange with transverse electric fields for synchronous waves because their electrons lack transverse velocities.

The plus sign in the expressions for the kinetic power of transverse waves indicates that excitation of a corresponding wave leads to a rise in the electron beam energy compared with that of an undisturbed beam. The a minus sign indicates the reverse process, that is, decreasing electron beam energy as part of it is extracted by the external electric field.

A synchronous wave with a complex amplitude R_{2-} has a positive kinetic power; in other words, its excitation is associated with the electron beam acceleration. For this reason, such a wave is usually called a fast synchronous wave (FSW), and the wave with the amplitude R_{2+} is called a slow synchronous wave (SSW).

2.4 About longitudinal and transverse waves

Dynamic longitudinal grouping effected by electric fields oriented parallel to the electron beam (see Fig. 2) was a natural step forward from classical electronic lamps (diodes, triodes, etc.) with a longitudinal electric field that ensured static control of the electron beam. In the small-signal approximation, bunching (compression) and rarefication of the space charge in the electron beam can be described in terms of its fast (+) and slow (−) waves [5, 12, 24, 26, 27] with the phase velocities

$$v_{\phi\pm} = \frac{v_z}{1 \mp \omega_q/\omega} , \tag{26}$$

where v_z is the mean (undisturbed) electron beam velocity and ω_q is the plasma frequency.

Space charge waves propagate inside an electron beam, that is, they are longitudinal electron-beam waves. Transverse waves (Fig. 3b) are associated with the transverse displacement and the transverse motion of the electron beam as a whole; in other words, they are transverse electron-beam waves.

Strictly speaking, the terminology of longitudinal waves is elaborated only in the small-signal approximation and for one-dimensional (infinitely wide) electron beams. In contrast, the notion of transverse waves is unrelated to restrictions on the signal level; this, however, refers in full measure to the filamentary beam model alone.

In the case of longitudinal grouping, the distribution of Coulomb fields produced by bunched charges in beams of finite diameter may be drastically distorted. The distortion is formally taken into account by the introduction of the so-called reduced plasma frequency that shows a nonlinear dependence on many factors, including the operational frequency, signal level, beam radius, radius of the metal drift tube, etc. [24, 26]. In other words, under real conditions, ω_q in Eqn (26) is nonlinearly dependent on all these parameters.

Expressions for phase velocities of cyclotron waves (14) and phase velocities of space charge waves (26) are outwardly similar. However, the former are unrelated to ω_q and determined by the cyclotron frequency value depending only on the magnetic flux density characterized by a fixed distribution along the axis of the device given by an external magnetic system.

Circular polarization of transverse waves in conjunction with the stability and predictability of their phase velocities ensures a high degree of selectivity of energy exchange between cyclotron/synchronous waves and external electromagnetic fields.

In certain cases, the filamentary model may be applied to an electron beam having a finite diameter. For a uniformly charged electron beam of a circular or rectangular cross section, there are no transverse Coulomb fields in the center of mass of this cross section (because they compensate each other) and the beam propagates as a single electron not involved in Coulomb interactions [16, 22, 23, 27, 29]. If the cross section remains undisturbed in the course of interaction, the technique of transverse waves developed for the filamentary beam adequately reflects the real picture. Such a situation occurs, for example, in a resonator with a uniform electric field (see also Section 3) regardless of the signal level up to the interception of the electron beam by the resonator bars. At a low level of the input signal, the transverse dimensions of the beam are frequently much larger than the cyclotron (Larmor) orbits.

Even in more general cases, consideration based on coupled transverse wave equations may be useful because it allows a relatively simple analysis of the physical picture of one type of interaction or another and the simultaneous evaluation of the limiting values of the parameters of interest (the maximum attainable efficiency, amplification factor, etc.). At the next stage, the results for the selected interaction can be checked and specified using numerical simulation techniques.

2.5 Numerical simulation. Helix-type discretization of the injected electron beam

Various 'big charged particle' models are used in vacuum microwave electronics to simplify numerical simulation procedures. The mechanism of interaction in a longitudinal grouping (see Fig. 2) is basically one-dimensional and therefore permits one to efficiently employ a one-dimensional model in the form of a sequence of charged disks interacting with each other and with external electromagnetic fields. A two-dimensional model (charged rings) makes it possible to consider the complicated processes associated with field inhomogeneities of technological origin along the radius of the beam that may cause it to stratify.

The transverse grouping discussed in this paper is in its physical essence a three-dimensional process, which implies

[1] We emphasize that this is true only for the part of electron flow kinetic power which that as a result of the interaction between the beam and the microwave field. For an unperturbed flow, $P_{1\pm} = P_{2\pm} = 0$ because $R_{1\pm} = R_{2\pm} = 0$, although $I_0 U_0 \neq 0$. Mathematical derivation of expressions (23)–(35) encounters no difficulty. The reader is referred to Refs [23, 24, 27, 28] for details.

that the relevant numerical simulation must also be three-dimensional. Nevertheless, the simulation procedure can be substantially simplified in selected cases [22, 23, 30].

We consider the motion of an electron labeled by i:

$$\frac{\mathrm{d}}{\mathrm{d}t}\,(m_i\,\mathbf{v}_i) = -e\left(\mathbf{E} + [\mathbf{v}_i\,\mathbf{B}]\right), \tag{27}$$

or

$$\frac{\mathrm{d}\mathbf{v}_i}{\mathrm{d}t} = -\frac{e}{m_0\gamma_i}\left(\mathbf{E} - \frac{\mathbf{v}_i}{c^2}\;\mathbf{v}_i\mathbf{E} + [\mathbf{v}_i\,\mathbf{B}]\right), \tag{28}$$

where

$$\gamma_i = \left(1 - \frac{|\mathbf{v}_i|^2}{c^2}\right)^{-1/2}$$

and, accordingly,

$$\mathbf{E} = \mathbf{E}_\mathrm{b} + \mathbf{E}_\mathrm{mw}\,, \quad \mathbf{B} = \mathbf{B}_\mathrm{b} + \mathbf{B}_\mathrm{mw} + \mathbf{B}_0\,,$$

where $\mathbf{E}_\mathrm{b}$ and $\mathbf{B}_\mathrm{b}$ are the electric field strength and magnetic flux density, respectively (the two fields being induced by the electron beam), $\mathbf{E}_\mathrm{mw}$ and $\mathbf{B}_\mathrm{mw}$ are the same quantities for the external microwave field, and $\mathbf{B}_0$ is the magnetic flux density of the external stationary magnetic field.

As in Section 2.3, z and t are assumed to be independent variables, which enables a transition from the description of single-electron motion to that of filamentary beam behavior (Fig. 3a), i.e.,

$$\zeta_i(z,t) = x_i(z,t) + \mathrm{i}y_i(z,t)\,, \tag{29}$$

$$\frac{\mathrm{d}}{\mathrm{d}t} = \frac{\partial}{\partial t} + v_{zi}\,\frac{\partial}{\partial z} \tag{30}$$

in (27) and (28).

Such filamentary electron beams may be used to describe a real electron beam of a finite diameter.

We discuss, by way of example, the interaction of a retarded circularly polarized traveling wave,

$$E_\perp = E_x + \mathrm{i}E_y = E_0 \exp\left[\mathrm{i}\,(\omega t - \beta z)\right],$$

$$E_z(\zeta,z,t) \approx \mathrm{Re}\left(\zeta^*\,\frac{\partial E_\perp}{\partial z}\right) = -\mathrm{Re}(\mathrm{i}\beta\,\zeta^* E_\perp)\,, \tag{31}$$

with an electron beam of a circular cross section being injected along this wave axis (i.e., the z axis in Fig. 4). The external stationary and uniform magnetic field B_0 is directed parallel to the same axis.

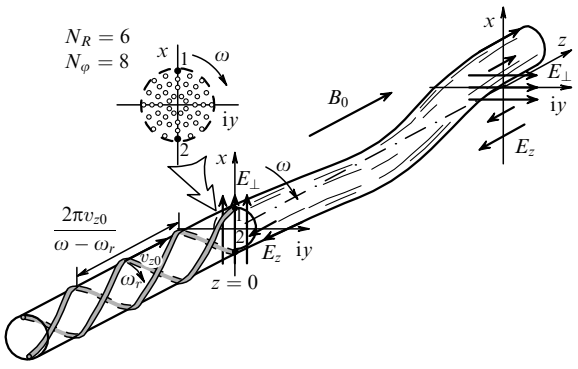

Figure 4. Helix-type discretization of the electron beam being injected.

We represent the electron beam being injected as a totality of partial (filamentary) beams. Each partial beam is assumed to be shaped as a spiral with the pitch

$$h = \frac{2\pi v_{z0}}{\omega - \omega_r}\,, \tag{32}$$

where v_{z0} is the beam longitudinal velocity and ω_r is the angular frequency of beam rotation around its axis under the action of the internal (radial) field of Coulomb forces.

For a uniformly charged electron beam volume,

$$\omega_r = \frac{\omega_\mathrm{c}}{2}\left(1 - \sqrt{1 - \frac{2\omega_\mathrm{p0}^2}{\omega_\mathrm{c}^2}}\right), \quad \omega_\mathrm{p0}^2 = \frac{e}{m}\,\frac{\rho_0}{\varepsilon_0}\,; \quad \omega_\mathrm{c} = \frac{e}{m}\,B_0\,, \tag{33}$$

where ρ_0 is the space charge density in the electron beam being injected. In such a model, the intersection point of each partial (filamentary) beam with the input plane $z = 0$ rotates in a circle with the angular frequency ω but remains motionless (stationary) with respect to the wave field phase in this plane; hence,

$$\frac{\partial v_{zi}}{\partial t} = 0\,, \quad \frac{\partial \rho_i}{\partial t} = 0 \tag{34}$$

for any partial beam and throughout the interaction region.

The boundary conditions can be written as

$$\zeta_i|_{z=0} = r_0\sqrt{\frac{2k-1}{2N_R}}\,\exp\left\{\mathrm{i}\left[\omega t + \frac{\pi}{N_\varphi}\,(2l+k)\right]\right\}, \tag{35}$$

where $\zeta_i = x_i(z,t) + \mathrm{i}y_i(z,t)$; $i = 1,2,\ldots,N$; $i = (k-1) + l$; $k = 1,2,\ldots,N_R$; $l = 1,2,\ldots,N_\varphi$; $N = N_R N_\varphi$; r_0 is the radius of the electron beam being injected; N_R is the number of rings; N_φ is the number of beams in each ring; and N is the total number of partial beams (usually 50 – 150);

$$\left.\frac{\partial\zeta_i}{\partial z}\right|_{x=0} = -\mathrm{i}\,\frac{\omega - \omega_r}{v_{z0}}\;\zeta_i|_{z=0}\,, \quad \left.\frac{\partial\zeta_i}{\partial t}\right|_{z=0} = \mathrm{i}\omega\zeta_i|_{z=0}\,. \tag{36}$$

Using the continuity equation, it is possible to write

$$\mathrm{div}\,\mathbf{j}_i + \frac{\partial\rho_i}{\partial t} = \mathrm{div}\,\mathbf{j}_i = \frac{\mathrm{d}}{\mathrm{d}z}\,(\rho_i v_{zi}) = 0 \tag{37}$$

for each partial beam i.e.,

$$\rho_i(z)\,v_{zi}(z) = \rho_i(0)\,v_{zi}(0) = \mathrm{const}\,, \tag{38}$$

where $\rho_i(z)$ and $v_{zi}(z)$ are the space charge linear density of a partial beam along the z axis and its longitudinal velocity, respectively.

Numerical simulation is feasible for any fixed moment of time because any change in time is equivalent to a turn of the reference frame about the z axis (see Fig. 4). In other words,

$$\frac{\partial}{\partial t} = \mathrm{i}\omega \tag{39}$$

in all equations for transverse coordinates and transverse velocities.

We emphasize that the spiral shape of partial beams is important here only for the electron beam being injected

($z < 0$), whereas the same beams demonstrate an arbitrary behavior inside the interaction region that can be described for both longitudinal and transverse groupings.

Also, it is clear that any other form of fields, besides (31), may be considered provided they rotate about the z axis with the frequency ω.

It is not unusual that the curvature radius of partial beams is much larger than the transverse dimension of the electron beam. In this case, the Coulomb field can be approximately calculated as the field of charged rods arranged tangentially to the partial beams at their intersection points with the plane $z = \text{const}$ and having the same linear charge density [22, 23, 30]:

$$E_{bxi} = -\frac{1}{2\pi\varepsilon_0}\sum_{k=1}^{N}\frac{|\sigma_k|\left[W_{1k}(x_i - x_k) - W_{2k}(y_i - y_k)\right]}{R_{ik}^2 + \delta r_0^2}\,,$$

$$E_{byi} = -\frac{1}{2\pi\varepsilon_0}\sum_{k=1}^{N}\frac{|\sigma_k|\left[W_{3k}(y_i - y_k) - W_{2k}(x_i - x_k)\right]}{R_{ik}^2 + \delta r_0^2}\,, \quad (40)$$

$$E_{bzi} = -\frac{1}{2\pi\varepsilon_0}\sum_{k=1}^{N}\frac{|\sigma_k|\left[W_{4k}(y_i - y_k) - W_{5k}(x_i - x_k)\right]}{R_{ik}^2 + \delta r_0^2}\,,$$

where

$$W_{1k} = A_{2k}^2 + A_{1k}^2 A_{4k}^2\,; \quad W_{2k} = A_{1k}A_{2k}(A_{4k}^2 - 1)\,;$$

$$W_{3k} = A_{1k}^2 + A_{2k}^2 A_{4k}^2\,; \quad (41)$$

$$W_{4k} = A_{2k}A_{3k}A_{4k}\,; \quad W_{5k} = A_{1k}A_{3k}A_{4k}\,;$$

$$A_{2k} = \frac{x_k}{|\zeta_k|}\,; \quad A_{1k} = \frac{y_k}{|\zeta_k|}\,; \quad |\zeta_k| = \sqrt{x_k^2 + y_k^2}\,;$$

$$A_{3k} = (1 - A_{4k})^{1/2}\,; \quad A_{4k} = \cos\psi_k\,; \quad \sigma_k = \rho_k A_{4k}\,; \quad (42)$$

$$\tan\psi_k = \frac{\omega|\zeta_k|}{v_{zk}}\,;$$

$$R_{ik}^2 = W_{1k}(x_i - x_k)^2 + W_{3k}(y_i - y_k)^2 - 2W_{2k}(x_i - x_k)(y_i - y_k)\,; \quad (43)$$

$\rho_0 = I_0/(Nv_{z0})$; I_0 is the electron beam current; and δr_0 is the minor addition introduced to eliminate singularities at $x_i \to x_k$, $y_i \to y_k$ and chosen to equal half the minimum distance between the partial beams in plane $z = 0$.

In the second example, a round electron beam in which all electrons initially (and similarly) rotate about the z axis is injected into a region with an axially symmetric and spatially alternating static magnetic (or electric) field, e.g.,

$$\mathbf{B} = \left(-\frac{x}{2}\frac{\mathrm{d}}{\mathrm{d}z}B_z\,,\ -\frac{y}{2}\frac{\mathrm{d}}{\mathrm{d}z}B_z\,,\ B_z(z)\right), \quad (44)$$

where $B_z(z, x = 0, y = 0)$ is the longitudinal component of magnetic induction along the z axis. The boundary conditions in the case of helix-type discretization then have the form

$$\zeta_i|_{z=0} = \left\{R_c\exp(i\varphi_0) + r_0\sqrt{\frac{2k-1}{2N_R}}\exp\left[i\frac{\pi}{N_\varphi}(2l + k)\right]\right\} \times \exp(i\omega t)\,, \quad (45)$$

where R_c, φ_0 are the radius and the initial phase of electron beam rotation as a whole, i.e., rotation, identical for all partial beams.

It can be seen from relations (44) and (45) that the track of each partial beam in the plane $z = 0$ rotates around the z axis and undergoes the time-invariable effect of the external axially-symmetric field. This accounts for the presence of all principal consequences of helix-type discretization (34), (38), (39) here.

These two simple examples give an idea of the relatively small but useful set of problems whose numerical simulation it is appropriate to perform using helix-type discretization of the injected electron beam.

3. Cyclotron-wave protectors (CWPs)

A resonator with a uniform transverse field in the interaction gap (Fig. 5) was the first device to be comprehensively studied (see, e.g., [22, 25, 31–34) and employed for the development of many microwave devices.

Unlike klystron-type resonators, this coupling device operates at large transit angles, i.e., in the interaction region

$$\frac{\omega l}{v_z} \geqslant (10-20)\,\pi\,, \quad (46)$$

where l is the length of the resonator bars that create a uniform transverse electric field.

In a microwave resonator (Fig. 5), only fundamental, operational oscillations are usually excited within the entire

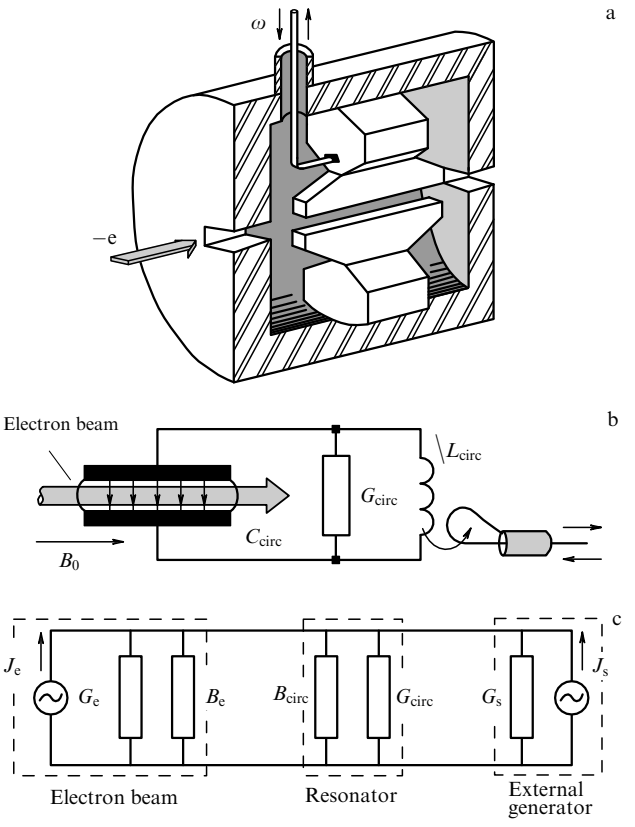

Figure 5. (a) Transverse-field resonator. (b, c) Equivalent schemes of an electron-beam resonator, J_e, J_s — currents induced by the electron beam and the source of an external signal; L_{circ}, C_{circ}, and G_{circ} — equivalent inductivity, capacity, and transmission of self-induced (active) losses in the resonator; B_0 — magnetic flux density of the external constant uniform magnetic field.

working frequency band, hence, the possibility of a simplified equivalent scheme in the form of a parallel oscillating circuit in which the electron beam passes through the interaction channel (Fig. 5b).

Equations for the scheme depicted in Fig. 5b may be written in analogy with those for coupled transverse waves (22) and the corresponding solution found in the analytic form (see, e.g. [20, 22, 25–27]). It is worth emphasizing that during interaction with a uniform electric field all electrons of the beam cross section are equally affected by this field, in other words, the shape of the cross section remains unaltered and the filamentary electron beam theory can be effectively applied at different microwave power levels.

The solution of the system of coupled transverse wave equations includes simultaneous computation of complex parallel transmissions introduced by transverse electron-beam waves:

$$Y_e = G_e + iB_e\,,$$

$$G_e = G_{e1+} + G_{e1-} + G_{e2+} + G_{e2-}\,, \qquad (47)$$

$$B_e = B_{e1+} + B_{e2-} + B_{e2+} + B_{e2-}\,.$$

Accordingly, the equivalent scheme presented in Fig. 5b may be reduced to the equivalent scheme depicted in Fig. 5c, which is more convenient for engineering calculations, it being known [20, 22, 25–27] that

$$G_{e1\pm} = \pm\frac{\omega}{\omega_c}\,G_0\left[\frac{\sin(\beta_\pm\theta_l/2)}{\beta_\pm\theta_l/2}\right]^2,$$

$$B_{e1\pm} = \mp 2\,\frac{\omega}{\omega_c}\,G_0\,\frac{\beta_\pm\theta_l - \sin(\beta_\pm\theta_l)}{(\beta_\pm\theta_l)^2}\,, \qquad (48)$$

$$G_{e2\pm} = \mp\frac{\omega}{\omega_c}\,G_0\left[\frac{\sin(\theta_l/2)}{\theta_l/2}\right]^2,$$

$$B_{e2\pm} = \pm 2\,\frac{\omega}{\omega_c}\,G_0\,\frac{\theta_l - \sin\theta_l}{\theta_l^2}\,, \qquad (49)$$

where $\beta_\pm = 1 \mp \beta_c/\beta_e$, $\theta_l = \beta_e l$,

$$G_0 = \frac{1}{8}\,\frac{I_0}{U_0}\left(\frac{l}{d}\right)^2,$$

I_0, U_0, l, d are the electron beam current, electron beam potential, resonator pad length, and interaction gap size, respectively.

In the case of cyclotron resonance ($\omega = \omega_c$), the amplitude of a fast cyclotron wave varies linearly over the interaction region while the beam is shaped as a straight line and rotates as a whole about the system axis (see also Fig. 6a).

The general picture of interaction can also be understood from the simplest qualitative reasoning. A linearly polarized uniform electric field in the interaction gap can be represented as the sum of two circularly right and left-polarized components and considered as a part of the wave field with an infinite phase velocity. The fast cyclotron wave is a circularly polarized wave, and its phase velocity at $\omega = \omega_c$ tends to infinity. It is known that two coupled waves having similar polarizations and phase velocities may effectively interact with each other.

For a slow cyclotron wave, condition (46) means that the interaction (energy exchange with this wave) is oscillatory in

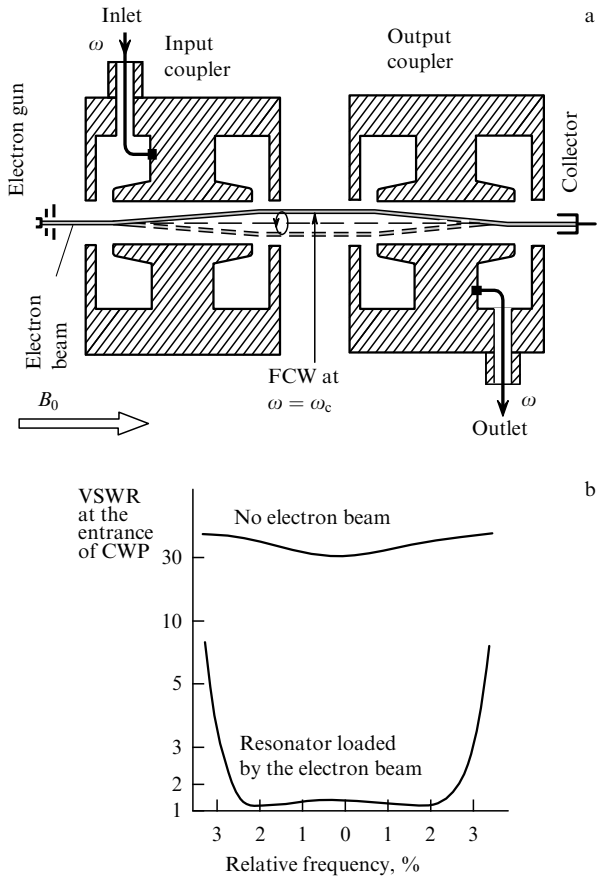

Figure 6. Schematic diagram of cyclotron-wave protector (a) and VSWR at the entrance of CWP (b).

nature; it is averaged and does not accumulate on the resonator pads. The energy exchange with synchronous waves is possible only at the periphery of the interaction region where the longitudinal component of the electric field E_z acquires a nonzero value.

If the power of energy exchange with an FCW at $\omega = \omega_e$ is arbitrarily assumed to be equal to unity, then it follows from Eqns (48) and (49) that the energy exchange with SCW is quantitatively below θ_l^{-2} and dose not exceed $4\theta_l^{-2}$ for SSW or FSW. Therefore, roughly speaking,

$$Y_e = G_e + iB_e\,, \quad G_e \approx G_{e1+}\,, \qquad B_e \approx B_{e1+}\,. \qquad (50)$$

In other words, a transverse electric field resonator interacting for a long time with an electron beam is a device in which selective energy exchange occurs between an FCW and this flow.

It follows from the electric circuit theory that the entire FCW power at the inlet of a resonator is extracted from the electron beam and transferred to the external circuit, with the transmiss

$$Y_{e1+} = Y_\Sigma^* - Y_{e1+}^*\,, \qquad (51)$$

where $Y_\Sigma = Y_e + Y_{circ} + Y_s$ is the summarized parallel transmission, $Y_{circ} = G_{circ} + i(\omega C_{circ} - \omega^{-1}L_{circ}^{-1})$ is the parallel transmission of the circuit, and $Y_s = G_s$ is the external load transmission counted into the parallel circuit that may usually be considered as active.

With expressions (50), this implies that

$$G_e = G_s + G_{circ}\,, \quad B_e = -B_{circ}\,. \tag{52}$$

In its turn, the power transmission from the signal source to the FCW is maximum at

$$Y_s = G_s = Y_\Sigma^* - Y_s^* \tag{53}$$

or

$$G_s = G_e + G_{circ}\,, \quad B_e = -B_{circ}\,. \tag{54}$$

These two conditions, (52) and (54), imply the necessity to compensate for the reactive constituent transmissions of the system. Choosing $\omega_0 = 1/\sqrt{L_{circ}C_{circ}} = \omega_c$, it is possible to have $B_e(\omega) = -B_{circ}(\omega)$ in a certain frequency range [20, 22, 35] where $B_e(\omega)$ and $B_{circ}(\omega)$ compensate each other.

In this case, maximum values of the coefficients of power transmission from the FCW to the external load (K_1) and from the external signal source to the FCW of the electron beam (K_2) are equal to each other and limited only by the amount of intrinsic Joule losses in the resonator:

$$K_1 = K_2 = 1 - \frac{G_{circ}}{G_e}\,. \tag{55}$$

In practice, each resonator is characterized by a quality factor $Q_0 \sim 700-1500$, dropping to $Q_L \sim 6-30$ under the load of an electron beam. Approximately,

$$K_1 = K_2 \approx 1 - \frac{Q_L}{Q_0} \quad (G_{circ} \ll G_e)\,. \tag{56}$$

At $Q_0 = 1000$ and $Q_L = 10-20$, the losses in a coupling device amount to $1-2\%$.

We now consider the diagram in Fig. 6a containing a sequence of two resonators loaded by a common electron beam and selectively interacting with an FCW. In the first resonator, a signal from the external generator is transferred to the FCW and in the second one, the same signal is extracted from the FCW and transferred back to the external circuit. In accordance with (56), the loss of the signal in such a system does not exceed several per cent. The initial noises contained in the FCW of the electron beam and associated with noise phenomena in the electron gun may be completely removed from the beam and dispersed over inner loads of the signal source and the resonator.

Part of the noises generated by the resonator itself (G_{circ} noises) may be expected to enter the signal channel (FCW at the outlet of the resonator). Due to this, the equivalent temperature of FCW noises

$$T_{1+} \approx \frac{Q_L}{Q_0}\,T_0 \tag{57}$$

(where $T_0 = 292$ K is room temperature) does not exceed about 6 K at $Q_0 = 1000$ and $Q_L = 20$.

A signal from the input generator enters the output one only with the electron beam. A forcible disruption of the flow by applying a negative potential to one of the electron gun electrodes results in the decoupling of the resonators and the damping of the signal between the inlet and the outlet by 100 dB; this provides reliable protection of the subsequent receiver cascades (see Fig. 1). For this purpose, it is possible to use the gun electrode that carries no current in the operational regime; in this case, the working time is of the order of several nanoseconds.

In the operating regime (in the presence of an electron beam), the resonator is loaded much heavier than in the absence of the flow:

$$G_e + G_{circ} \gg G_{circ}\,. \tag{58}$$

Therefore, in the latter case, the main part of the power is reflected at the inlet of the CWP, thus enabling it to effectively sustain high overloads by input signals. In real structures, the voltage standing wave ratio (VSWR) at the inlet of the CWP (Fig. 6b) is $1.05-1.2$ in the presence of an electron beam and increases to 30 in its absence [34–37]. The maximum allowable input power level is normally as high as 500 W in the continuous regime and 500 kW in the pulsed regime.

Cyclotron-wave protectors successfully work both under forced current commutation conditions and in the automatic regime. At a low external signal level, unless it falls below a certain threshold level (usually about 1 mW), the electron beam rotates as a whole at the angular frequency $\omega = \omega_c$ without coming in contact with the input resonator bars (Fig. 6a). However, it becomes intercepted by the bars as the radius of rotation gradually increases with increasing the input power; as a result, the beam is deposited in the input resonator and does not enter the second (output) one. At a high input signal level, the beam current is totally intercepted under the action of the transverse electric field created by the resonator bars on the side of the electron gun (i.e., upon its first encounter with the microwave field). As in the case of forced commutation, the load introduced into the resonator by the electron beam disappears and the main part of the input signal power is reflected at the inlet of the CWP (Fig. 6b).

It is worth mentioning one simple but important feature of CWPs. The value of the output signal from a CWP cannot in principle be higher than that permitted by the gap between the output resonator pads. This accounts for the absence of the so-called leakage power peak that exists in many protective devices and creates many unwanted problems in subsequent cascades of a microwave receiver.

Modern state of the art technologies provide an operating frequency range of a CWP of around 10% at 3 GHz, 5% at 10 GHz, and over 2% at 35 GHz [34–37]. The electron beam current is usually $50-150$ μA at $6-50$ V. Interception of such low-energy beams in the resonator poses no serious problems. The characteristic time of restoration after overloads (i.e., time of transition from the protective regime to the linear amplification regime) is normally less than 10 ns; it is determined by the relaxation time of oscillations in the input low-quality resonator and the electron flight-of-time between the resonators.

Figures 7a and 7b show CWPs designed by the Istok Corporation to be operated in the 9 GHz and 35 GHz ranges.

4. Cyclotron-wave parametric amplifiers (CWPAs)

If the two resonators shown in Fig. 6 are separated by a section increasing the FCW amplitude, the resulting amplifier has a low noise level (because FCW noises are removed in the input coupler) and retain all the protective properties of a

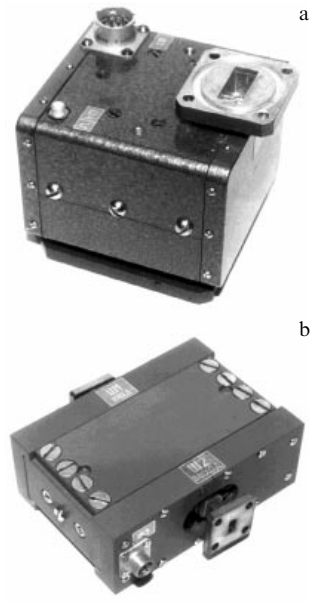

Figure 7. CWPs operated in the 9 GHz (a) and 35 GHz (b) ranges (Istok Corporation).

CWP. A resonator with the quadrupole electric field fed from an external pumping source with the frequency about double the cyclotron frequency [26, 27, 38, 39] may be used to construct the electron-beam parametric amplifier schematically depicted in Fig. 8.

We consider a quadrupole electric field with the potential

$$V(x,y,t)=\frac{V_0}{a^2}\,(x^2-y^2)\cos\omega_{\rm p}t\,,$$

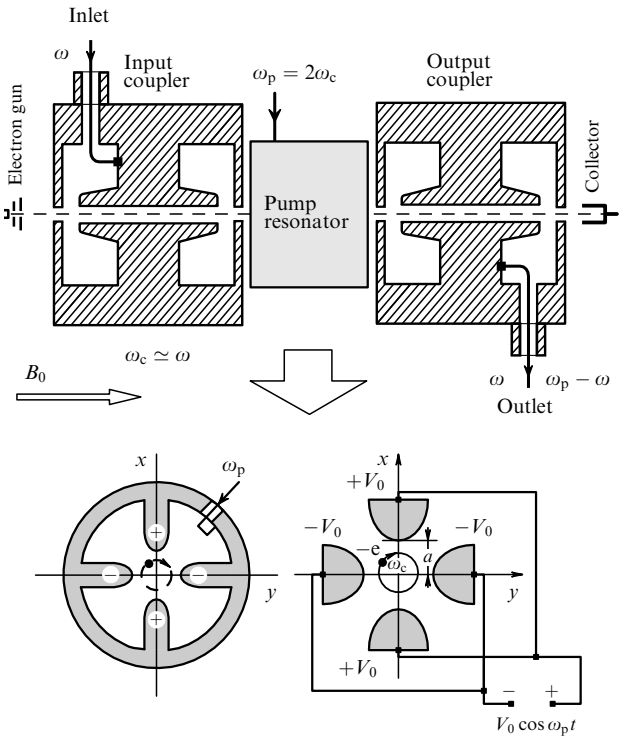

Figure 8. Schematic diagram of a degenerate cyclotron-wave parametric amplifier.

where V_0 is the potential of quadrupole bars, a is the minimal distance between the bars and the z axis, and $\omega_{\rm p}$ is the angular frequency of the pump generator.

An electron entering the quadrupole region with the phase $-\pi/4$ or $3\pi/4$ is accelerated by the quadrupole field (see Fig. 8). After the half-period of cyclotron rotation, the electron again undergoes acceleration because the pumping frequency is twice the cyclotron frequency, etc. The radius of electron rotation around the axis monotonically increases. By the very same reasoning, an electron entering the quadrupole region with the phase $\pi/4$ or $5\pi/4$ is monotonically decelerated. Of special interest are adiabatic fields where the radius of rotation varies insignificantly during the time of one electron revolution around the z axis.

Based on Eqns (22) and the above expression for $V(x,y,t)$, it can be shown that from the standpoint of the wave concept, phase selectivity of amplification processes in the pumping quadrupole region is responsible for the appearance of an additional wave in the course of amplification of the fundamental wave. In other words, a FCW at the signal frequency ω gives rise to another FCW at the difference (idler) frequency $\omega_{\rm i}=\omega_{\rm p}-\omega$. The amplitude of the former wave increases in accordance with the law $\cosh(\mu\beta_{\rm c}z)$ and that of the latter in accordance with the law $\sinh(\mu\beta_{\rm c}z)$, where μ is the minor amplification parameter,

$$\mu=\frac{eV_0}{2ma^2\omega_{\rm c}^2}\,.$$

The difference (idler) channel also exists at the inlet of a CWPA. A fast cyclotron wave entering the quadrupole region undergoes acceleration and simultaneously gives rise to an idler wave, whose frequency $\omega_{\rm i}=\omega_{\rm p}-(\omega_{\rm p}-\omega)=\omega$ corresponds to the signal channel frequency at the exit from this region.

Because $\omega_{\rm p}=2\omega_{\rm c}$ and $\omega_{\rm c}\approx\omega$, the idler channel frequency is close to that of the signal channel, $\omega_{\rm i}\approx\omega$. The frequencies of the signal and idler channels are always symmetric with respect to $\omega_{\rm p}/2$. Such parametric amplifiers are usually referred to as degenerate on quasidegenerate ($\omega_{\rm i}\approx\omega$).

It is important to discuss what to do with the idler channel. The alternative variants are as follows: (1) not to use it at all, (2) to use it in the optimal way, (3) to substantially increase its frequency or (4) to eliminate (compensate) the idler channel.

1. If the idler channel is disregarded, as is appropriate in many applications, the equivalent temperature of CWPA intrinsic noises increases due to additional noises incoming at the idler channel frequency from the signal source (antenna),

$$T_{\rm CWPA}=\frac{G_{\rm circ}}{G_{\rm e}}\,T_0+\left(1-\frac{G_{\rm circ}}{G_{\rm e}}\right)T_{{\rm A},\,\omega_{\rm p}-\omega}\,, \qquad (59)$$

where $T_{{\rm A},\,\omega_{\rm p}-\omega}$ is the equivalent temperature of noises coming from the signal source (antenna) at the idler frequency.

The second term in formula (59) implies that noises arriving from the signal source (antenna) at the idler frequency in the course of parametric acceleration are totally pumped into the signal frequency channel, while the electron beam noises at the idler frequency are effectively eliminated in the second coupling device. It is important to emphasize that $T_{{\rm A},\,\omega_{\rm p}-\omega}$ may also be significantly smaller than T_0, e.g., in CWPAs used for cosmic radiolocation and communication.

2. On the other hand, when a noise-like signal with a continuous spectrum has to be received (e.g., as in radio-

astronomy), both channels are used and the maximum sensitivity of the CWPA is realized, because

$$T_{\mathrm{CWPA}} = \frac{G_{\mathrm{circ}}}{G_{\mathrm{e}}}\, T_0 \qquad (60)$$

can be below 10 K.

Moreover, in certain systems, including some radiolocation stations (RLSs), electron-paramagnetic resonance (EPR) and nuclear magnetic resonance (NMR) spectrometers, the signal being produced can be formed such that it reaches the inlet of the receiver with a CWPA simultaneously through the signal and idler channels.

Finally, one more possibility is worth mentioning. The output signal from a CWPA containing two oscillations at the signal and idler frequencies may be represented as a single oscillation at the frequency $\omega_{\mathrm{p}}/2$ with variable amplitude and phase, the latter practically taking only two discrete values differing by π radian [22, 26, 40]. This effect is usually called the phase quantization effect in degenerate parametric systems. Phase discreteness makes it possible to employ the phase detection procedure using part of the signal from the pump generator as the reference signal after dividing its frequency by two and determining the optimum phase. In the phase detection procedure, unlike amplitude detection techniques (quadratic and linear), the information is extracted from both the amplitude and the phase of the signal being received. This is an advantage, especially noticeable at a small signal-to-noise ratio. The aforesaid is confirmed by laboratory experiments with CWPA [22].

3. Nondegenerate parametric amplifiers with an enlarged multiplicity of pumping frequency (e.g., $\omega_{\mathrm{p}} = 5\omega_{\mathrm{c}}$, $\omega \approx \omega_{\mathrm{c}}$, $\omega_{\mathrm{i}} \approx 4\omega$) are feasible in principle [20] but are very complicated in terms of construction and have never found wide application.

4. The idler channel can be obviated (compensated) by using two electron beams (Fig. 9) passing through the common input and output coupling devices but across different quadrupole fields equal in intensity but shifted in phase by π radians [20, 22, 41]. The wave phase at the idler frequency, unlike the signal wave phase, depends on the pump field phase; therefore, idler waves in the output coupler are out of phase; they compensate one another without interacting with it, remain in the electron beam, and move to the collector. Additional measures are needed in a two-beam parametric amplifier to remove noises associated with cyclotron waves, e.g., the use of two independent resonators as shown in Fig. 9 or a single resonator correlating these noises by counterphase electric fields [20, 22, 41]. The equivalent temperature of intrinsic noises in a two-beam amplifier is determined by extrinsic load noises from additional resonators. These loads may have a compact structure and be additionally cooled if necessary.

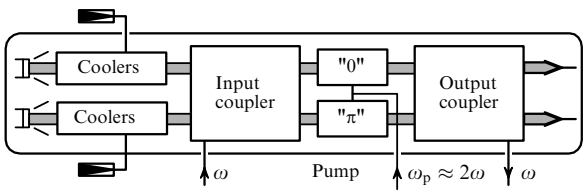

Figure 9. Schematic of a two-beam parametric amplifier with a suppressed idler channel.

Instead of additional resonators in a two-beam parametric amplifier, it is possible to use an adiabatically decreasing magnetic field to reduce cyclotron wave noises, as is usually done in CWESAs (see Section 5).

Here are, briefly, a few specific features of parametric amplification processes in CWPAs.

• Amplitudes of signal and idler cyclotron waves increase in a quadrupole pump field, either wave being a fast one. In accordance with (23) and (24), this means that the electron beam energy also increases due to the energy coming from an external pumping source.

• It can be shown using (6) that the result of energy exchange between cyclotron orbits and a quadrupole field during resonant ($\omega_{\mathrm{p}} = 2\omega_{\mathrm{c}}$) and adiabatic ($\mu \ll 1$) interactions is independent of the displacement of the orbit center with respect to the field axis [20, 22, 42]. This means that amplification of cyclotron waves is independent of the synchronous wave amplitude. Also, important from the technological standpoint is the conclusion that coaxiality of the quadrupole field and the remaining device is inessential.

• The electron beam at the output of the electron gun has cyclotron orbits determined by the velocity dispersion of electrons emitted from different points at the heated cathode surface. At the inlet of a coupling device, a new rotation common to all electrons of the beam cross section and associated with the external signal is added. Internal thermal oscillations in the electron beam caused by the velocity dispersion at the cathode surface can be conveniently described in a coordinate system whose origin coincides with the center of mass of the beam cross section. Modulation caused by the external signal has the form of the motion of the center of mass of the beam cross section (the beam as a whole) in the laboratory reference frame whose origin is coincident with the axis of the device. For a round electron beam uniformly charged over the cross section, the Coulomb fields in the center of mass are compensated and it propagates as an individual electron not involved in Coulomb interactions. In other words, the internal Coulomb fields do not necessarily influence amplification of a useful informative signal unless the beam cross section and the charge distribution in it are distorted.

• In contrast, inner thermal cyclotron orbits undergo the action of the radial field of Coulomb forces that on the one hand cause the electron beam to slowly rotate about its axis and on the other hand are responsible for dynamic detuning between the actual electron rotation rate and $\omega_{\mathrm{p}}/2$ [29, 42]. This hampers the growth of inner (thermal) cyclotron orbits in a high-frequency quadrupole field. Thus, the radial field of the Coulomb forces present in a round electron beam is useful and may interfere with and even prevent expansion of the beam cross section during its interaction with the quadrupole pump field [20, 22, 29, 42].

• Noise from low-power pump generators of CWPAs is usually very small (below -120 dB with respect to the carrying one) and does not have any apparent effect on the noise factor of a given parametric amplifier.

On the whole, the processes of parametric amplification of the FCW of the electron beam in a quadrupole pump field are rather readily and reliably realized under practical conditions. The amplification coefficient of 25–30 dB and more is easily achieved at a low level of intrinsic noises of the CWPA.

Figure 10 shows one of the first commercial CWPAs developed under the guidance of S P Kantyuk. The size of

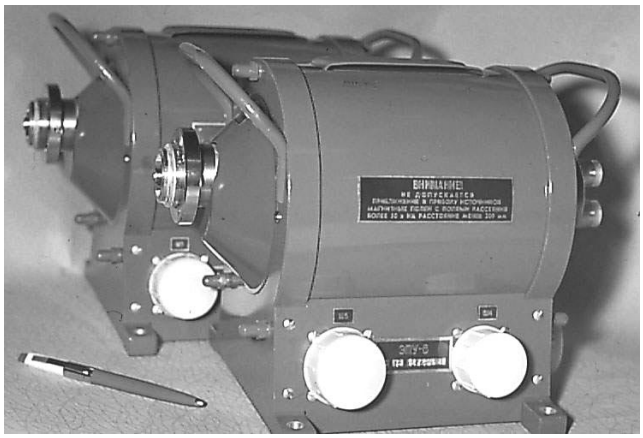

Figure 10. One of the first commercial CWPAs developed by S P Kantyuk (Istok Corporation, Russia).

the input coaxial connector of this low-noise instrument is enlarged to allow a pulsed microwave power of 500 kW to be delivered to the inlet.

Up-to-date technologies allow placing a pump generator inside the device casing and using compact magnetic systems with highly efficient samarium – cobalt permanent magnets to considerably reduce the volume, weight, and energy consumption of the CWPA (to 1.5 – 3 W of the direct current power at low feeding voltage).

5. Cyclotron-wave electrostatic amplifier (CWESA)

Apart from the parametric quadrupole zone of amplification (see Fig. 8), it is possible to use an electrostatic structure whose potential varies periodically along the z axis [20, 26, 36, 37, 43]. An electron propagating along the z axis at a speed v_z 'senses' a time-variable electric field with the angular frequency

$$\omega_e = \frac{2\pi}{L_s}\, v_z\,, \tag{61}$$

where L_s is the spatial period of the electrostatic field.

If this field contains a quadrupole component, the amplitudes of cyclotron waves increase provided the resonance condition $\omega_e = 2\omega_c$ is satisfied.

Modern CWPs and CWESAs (Fig. 11a) usually employ ribbon electron beams [34 – 37, 44, 45] that allow increasing the load on the input and output coupling devices and thereby broadening the operating frequency band. Ribbon electron beams are normally used in conjunction with a flat electrostatic periodic system (Fig. 11b). The field potential inside such an amplifying system can be approximately written as

$$V(x,z) \approx \frac{V_s}{b^2}\, x^2 \cos\frac{2\pi}{L_s}\, z = \frac{V_s}{2b^2}\,(x^2 - y^2)\cos\frac{2\pi}{L_s}\, z + \frac{V_s}{2b^2}\,(x^2 + y^2)\cos\frac{2\pi}{L_s}\, z\,, \tag{62}$$

where b is the normalization parameter of the length dimension.

Thus, a plane-periodic field may be represented as the sum of two spatially periodic fields, one quadrupole and the other axially symmetric. Resonance conditions, $\omega_e = 2\omega_c$ for one and $\omega_e = \omega_c$ for the other field, are different. It is easy to see that whenever the former condition is satisfied, cyclotron waves are actively coupled between themselves and increase; when the latter condition is satisfied, the cyclotron waves are actively coupled with synchronous ones and grow along the z axis.

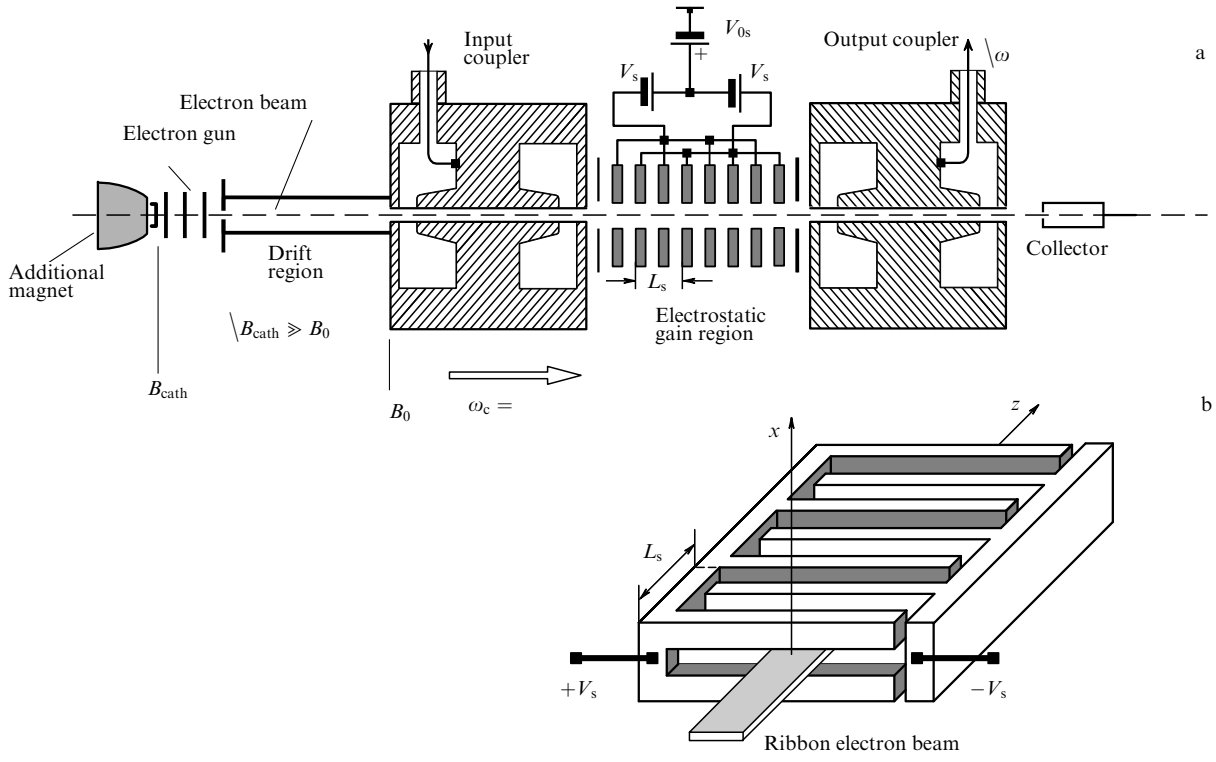

Figure 11. Schematic diagram of a cyclotron-wave electrostatic amplifier (a) and a plane-periodic electrostatic gain structure (b).

The mean energy exchange with an electrostatic quadrupole field is always zero and the growth of the FCW (positive kinetic power) is inevitably associated with the growth of the SCW (negative kinetic power). In the case under consideration, an SCW at the signal frequency ω plays the role of a difference (idler) wave that arose in the high-frequency quadrupole field during parametric amplification (see Section 4). This situation can also be illustrated from the formal standpoint. For an electrostatic amplifying element, it may be assumed that $\omega_p = 0$, and hence $\omega_i = \omega_p - \omega = -\omega$. Then, it follows from (13) and (20) that an FCW at the frequency $-\omega$ is SCW at ω.

In the course of electrostatic amplification, the amplitudes of FCW and SCW increase as $\cosh(\mu\beta_c z)$ and $\sinh(\mu\beta_c z)$, respectively, where μ is the amplification parameter,

$$\mu = \frac{eV_s}{4mb^2\omega_c^2} \ll 1 .$$

In accordance with this interaction scheme, an SCW of an electron beam at the inlet of the amplification zone must increase in accordance with the law $\cosh(\mu\beta_c z)$ and lead to the appearance of an FCW with the amplitude growing as $\sinh(\mu\beta_c z)$.

Due to this, noises associated with both fast and slow cyclotron electron-beam waves enter the signal channel.

It is known that the equivalent temperature of cyclotron wave noises at the cathode surface is [46]

$$T_{1\pm} = \frac{B_0}{B_{cath}} T_{cath} = \frac{\omega}{\omega_{c,cath}} T_{cath} , \quad (63)$$

where T_{cath} is the cathode temperature (Kelvin scale), $\omega_{c,cath} = (e/m) B_{cath}$ is the cyclotron frequency at the cathode surface, B_{cath} and B_0 denote the magnetic flux density at the cathode surface and in the operating region, and ω is the signal frequency.

It can be shown using (22), (23), and (43) that kinetic powers of cyclotron waves are preserved when the magnetic field adiabatically decreases:

$$P_{1\pm} = \text{const}_{1\pm} . \quad (64)$$

Therefore, when choosing $B_{cath} \gg B_0$ and then adiabatically decreasing it to a resonant value, the minimal equivalent temperature of intrinsic noises in CWESAs (Fig. 11a) is determined by the SCW noise level:

$$T_{CWESA} = T_{1-} = \frac{B_0}{B_{cath}} T_{cath} = \frac{\omega}{\omega_{c,cath}} T_{cath} . \quad (65)$$

If it is assumed that $T_{cath} \approx 700$ K and $\omega_{c,cath}/(2\pi) \approx 50$ GHz, then T_{CWESA} is approximately 42 K for the operating frequency 3 GHz and 140 K for the frequency 10 GHz.

The physical mechanism of cyclotron wave noise attenuation in an adiabatically decreasing magnetic field is rather simple. The radial component of the magnetic flux density for each cyclotron orbit,

$$B_r = -\frac{r}{2}\left(\frac{dB_z}{dz}\right)_{x=y=0} , \quad (66)$$

interacts with the longitudinal velocity of an electron and tangential velocity of its cyclotron rotation, thus leading to the appearance of two components of the Lorentz force. One of them slows down rotational motion of the electron and the other increases its longitudinal velocity. The total energy of each cyclotron orbit is conserved; part of the cyclotron rotation energy is converted into additional energy of longitudinal motion. For an adiabatically varying magnetic field, this process is on the average independent of the displacement of the orbit center with respect to the magnetic field axis.

We also recall that the ratio of the oscillation energy to the eigenfrequency for any linear oscillator is invariant in the case of adiabatic alteration of the parameters. Therefore, for each cyclotron orbit,

$$\frac{E}{\omega} = \frac{1}{\omega_c} \frac{mr_c^2\omega_c^2}{2} = \text{const} . \quad (67)$$

Comparison of Eqns (67) and (23) confirms the validity of (64) because $|R_{1\pm}|$ should be used instead of r_c for the center of mass of the beam cross section (Fig. 3b).

Realization of the principle of FCW amplification in an electrostatic quadrupole field encounters a number of additional physical and technical problems.

• The pitch of an electrostatic structure in the shortwave segment of the centimeter wavelength region necessary for resonant interaction,

$$L_s = \frac{2\pi}{\omega_e} v_z , \quad (68)$$

proves to be too small at the electron beam velocities v_z that are normally used in resonator couplers (potential 10 – 50 V. This dictates the necessity of raising the velocity of the electron beam in the amplifying element region by increasing the potential V_{0s} (Fig. 11a) to 150 – 200 V and higher. This inevitably leads to the appearance of beam acceleration and deceleration zones in front of and behind the amplifying element.

• Amplification of cyclotron waves (cyclotron orbits) in an electrostatic system decelerates the beam, i.e., decreases its longitudinal velocity, lowers effective frequency (61), and violates the resonance condition $\omega_e = 2\omega_c$; this, in turn, may restrict the amplification factor [47]. Moreover, amplification of thermal cyclotron orbits existing in the electron beam at the outlet of the electron gun interferes with the amplification of the useful signal even at its low levels.

• Phase selectivity of an electrostatic quadrupole field accounts for the fact that acceleration of thermal cyclotron orbits not only increases dispersion of electron longitudinal velocities but also causes a change in their distribution function. This, in turn, leads to the reflection of electrons in the beam acceleration and deceleration zones [48] with subsequent current deposition and enhanced noise levels. The resultant dispersion of velocities may also influence signal demodulation in the output resonator [49].

These effects make practical realization of high amplification factors, especially in the shortwave segment of the centimeter wavelength range, difficult. This has led to the construction of so-called electrostatic combined amplifiers (CWESCAs) with the electron amplification coefficient 10 – 15 dB, which is further increased by 10 – 15 dB using an additional transistor amplifier placed inside the CWESCA casing.

It should also be emphasized that these effects are absent during parametric amplification of cyclotron waves in a high-frequency quadrupole pump field (see Section 4); in this sense,

the mechanism of parametric amplification is simpler and can be more reliably realized for practical purposes.

That is why two-beam parametric amplifiers with the suppressed idler channel have good prospects for future use. Unlike the amplifier shown in Fig. 8, they have no additional resonators but contain a cooling system for cyclotron waves in the adiabatically decreasing magnetic field.

The processes of wave amplification in spatially periodic axially symmetric electrostatic fields [the second term on the right-hand side of (62)] were also considered in the literature [50 – 52]. Such devices are not included in the class of low-noise amplifier, however.

By way of example, Figure 12 shows the general view of an industrially manufactured version of a CWESA developed by the Istok Research and Production Corporation; it is operated at the average working frequency 4 GHz.

Selected parameters of CWESAs and CWESCAs are presented in the Table.

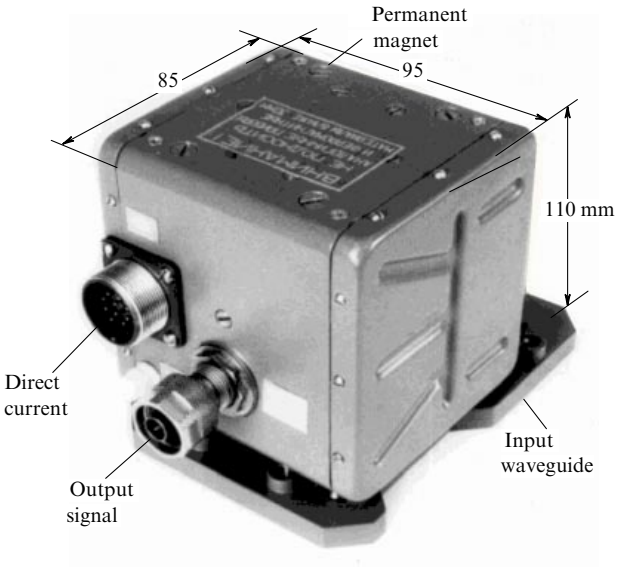

Figure 12. Electrostatic amplifier with the mean operating frequency 4 GHz (Istok Corporation). Pin connector serves to connect the amplifier to low-power DC sources.

Table. Certain parameters of CWESAs/CWESCAs

Mean operating frequency, GHz	0.2 – 11
Operating frequency range*, %	5 – 10
Noise factor*, dB	0.6 – 4
Gain, dB	20 – 25
Dynamic range ** (input signal), μW	10
Amplitude – phase noise at a frequency shift of 1 kHz, dB Hz^{-1}	−120
Allowed input microwave power level, pulsed and average, kW	up to 20 – 500 up to 2 – 5
Protection of subsequent receiver cascades, dB	60 – 120
Leakage power peak, mW	< 0.1
Restoration time after microwave overload***, ns	2 – 20
Consumed DC power, W	1 – 2.5
Time-lag after connection with power sources, s	< 1
Weight*, kg	0.5 – 5

* Depends on operating frequency.
** Additionally: + 20 dB of dynamic range extension in terms of power (up to 1 mW) by decreasing the voltage of the amplifying structure.
*** Depends on the impact pulse shape and intensity.

6. Tunable CWESA filter

Some technical applications require a narrow-band electrically tunable amplifier filter to be used at the inlet of radio receiving systems. On the one hand, such filters must have a sufficiently low level of intrinsic noises but, on the other hand, a broad dynamic range in conjunction with the ability to sustain high overloads by input signals and the reliable protection of subsequent receiving circuits against such overloads.

Cyclotron wave parametric and electrostatic amplifiers (see Sections 4 and 5) meet these requirements but contain input and output resonator couplers; also, their operating frequency cannot be electrically readjusted. A natural question arises as to the possibility to substitute resonators by distributed electrodynamic systems while preserving the passive character of energy exchange with the electron beam and equally high selectivity of interaction with its working (fast cyclotron) wave alone.

A schematic representation of a tunable CWESA filter is given in Fig. 13a. In this device, the electron beam interacts with the input and output coupling systems, each serving as a slow-wave structure (SWS). In the former, an input signal is pumped under certain conditions into an FCW of the electron beam; having passed the amplification system, the signal is extracted in the second coupler. The mechanism of formation of intrinsic low-level noises (high magnetic flux density at the cathode surface with its subsequent adiabatic decrease) and the principle of amplification (in the periodic electric field) are the same as in an ordinary CWESA (see Section 5).

In choosing a concrete SWS for the coupling device of a tunable CWESA filter, it is important that the transverse field of the working spatial harmonic in the interaction channel be sufficiently intense and uniform. On the contrary, the long-

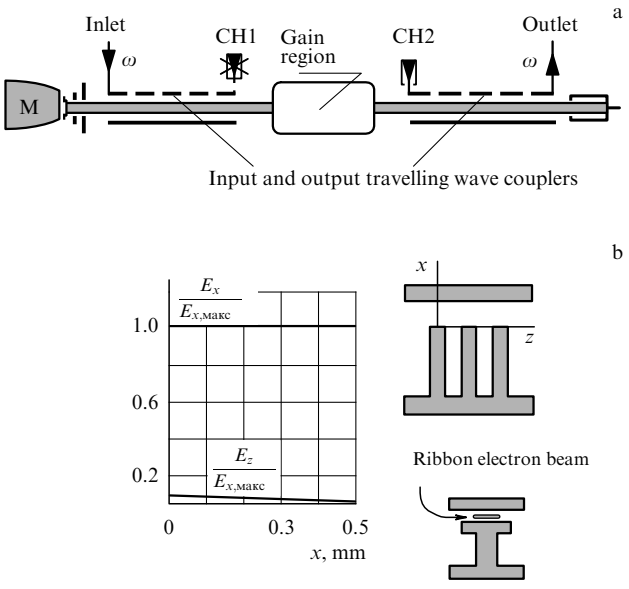

Figure 13. Schematic of a tunable SWESA filter (a) and electric field distribution in the comb interaction channel (b).

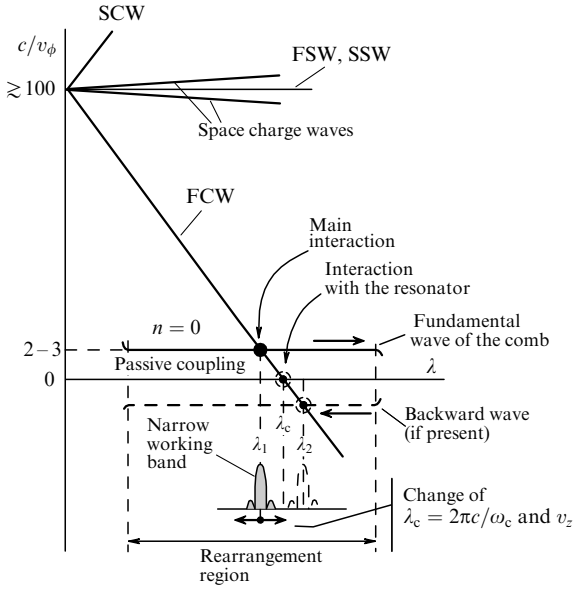

Figure 14. Dispersion characteristics of electron beam waves and the zero spatial harmonic of the comb.

itudinal electric field in the same region must be relatively weak. Calculations based on the available expressions for SWS fields [6, 53] indicate that in this situation, using a well-known one-row flat comb having the most intense and uniform transverse electric field of the zero spatial harmonic ($n = 0$) (Fig. 13b) shows great promise.

Figure 14 represents dispersion dependences of the deceleration coefficient $c/v_\phi(\lambda)$ for electron beam and SWS waves, where c is the phase velocity of the respective wave and $v_\phi(\lambda)$ is the wavelength in free space. If the beam longitudinal velocity is chosen to be sufficiently small (with the accelerating potential below 25 V), then $c/v_{z0} = c/v_\phi(0) \geqslant 100$ and phase velocities of synchronous waves, slow cyclotron waves, and spatial charge waves are significantly different from the phase velocity of SWS waves. In other words, these waves can selectively interact with the FCW of the electron beam at $\lambda = \lambda_1$ (see Fig. 14). The deceleration coefficient for the fundamental spatial harmonic wave ($n = 0$) in the comb should be chosen to equal 2–3. For the fundamental spatial harmonic, the phase change slope in a range-retuned amplifier is low enough ($c/v_\phi(\lambda) \approx$ const for $n = 0$), which is of value for many technological applications.

The theoretical analysis of energy exchange between an electron beam and the field of a distributed coupling element amounts to simultaneously solving the equations for the beam waves and the coupler. Using the technique of coupled waves and disregarding noninteracting ones (see Fig. 14), it is possible to derive a known system of equations describing the typical passive energy exchange between an electron beam FCW and a SWS wave (see, for instance [25]). In the case of the exact phase velocity synchronism of interacting waves at

$$L_{\text{dip}} = \frac{\pi}{2|k|}, \tag{69}$$

where $|k|$ is the passive wave coupling coefficient [25], complete energy exchange is realized, that is, all FCW energy is transferred to the SWS and vice versa. In a more general case, the power transmission coefficient [25]

$$F_P(\omega) = \frac{|k|^2 \sin^2\left(\sqrt{(\beta_0 - \beta_{1+})^2/4 + |k|^2}\, L_{\text{dip}}\right)}{(\beta_0 - \beta_{1+})^2/4 + |k|^2}, \tag{70}$$

where β_0 and $\beta_{1+} = \beta_e - \beta_c$ are the SWS wave and FCW propagation constants, respectively, is frequency-dependent and determines filtration characteristics of the distributed coupling device. The width of the transmission band is essentially dependent on coefficient $|k|$. The band broadens with growing $|k|$ and vice versa. This band is usually of the order of 1% but can be electrically readjusted within the SWS transparency band by varying the magnetic flux density and (or) beam potential (see Fig. 14).

The input and output couplers may be subject to matched loads (CH1 and CH2 in Fig. 13a) that absorb reflected (backward) SWS waves. If the backward waves are still present for one reason or another, the synchronism and the interaction with the FCW additionally occur at $\lambda = \lambda_2 > \lambda_c$, and therefore, the second transparency band appears (see Fig. 14).

In the absence of the CH1 load (Fig. 13a), when the electron beam is intercepted at a high-level input signal, a major part of its power is reflected from the end of the input SWS back to the input circuit of the device. Therefore, as in the devices described in preceding sections (CWPs, CWPAs, CWESAs), the inlet of the CWESA filter sustains relatively high input power levels, thus ensuring the reliable protection of subsequent receiver circuits. At the same time, it should be borne in mind that in the absence of CH1, the signal corresponding to $\lambda = \lambda_2$ in the reception regime enters the FCW electron beam in the input SWS but does not appear at the outlet of the CWESA filter because it is extracted from the flow in the output SWS and absorbed by the matched CH2 load.

An experimental version of the CWESA filter [22] has been tested at the following parameters of the comb and the electron beam: height of the comb tooth 7 mm, tooth width 4 mm, tooth thickness 0.6 mm, comb pitch 1.6 mm, gap between the teeth and the metal plane (interaction gap) 0.5 mm, $L_{\text{dip}} \approx 50$ mm at the electron beam current 150 μA and accelerating potential 13 V. Such a comb effectively interacted with electron beams in good agreement with the theory. Attenuation of the signal inside the filter when the amplification zone was switched off was only 0.1–0.3 dB, the width of the transmission band was of the order of 1% ($\lambda = 6$ cm), and the retuning region was over 20%. The last figure is presented here by way of illustration because no attempt was made in the present experiment to optimize this parameter; it was determined by the correlation band of the input and output coaxial lines with the corresponding combs.

Of certain interest are CWESA filters with combined interaction in which the amplification zone forms a single whole with the coupling devices. In this case, the SWS cannot be a monolithic structure; rather, it must be a more complicated construction consisting, for example, of two 'subsystems' isolated in terms of direct current, inserted into each other, and having different potentials. For a high-frequency (microwave) constituent, such a combined SWS looks like an ordinary two-row comb while the electrical isolation of the subsystems permits simultaneously applying a plane-periodic electrostatic pump field to the electron beam [22, 24].

In conclusion, it is worth noting that the removal of the amplification zone from the scheme in Fig. 13a gives a self-sufficient tunable narrow-band protective device in which attenuation of cyclotron wave noises in the adiabatically decreasing magnetic field is no longer necessary. Such a tunable protector may prove to be of great value for many technological applications in the future.

7. Circularly polarized traveling wave tube

We now consider a promising possibility to develop an amplifier in the form of a circularly polarized traveling wave tube (CPTWT).

We suppose that a slow circularly polarized traveling wave of the form

$$E_\perp = E_x + \mathrm{i}E_y = E_0 \exp\left[\mathrm{i}(\omega t - \beta_1 z)\right], \qquad E_z(\zeta, z, t) \approx \mathrm{Re}\left(\zeta^* \frac{\partial E_\perp}{\partial z}\right) = -\mathrm{Re}(\mathrm{i}\beta_1 \zeta^* E_\perp), \tag{71}$$

(where $\zeta = x + \mathrm{i}y$ is the complex transverse coordinate) propagates along the z axis and that a filamentary electron beam is injected along the axis of this wave with the velocity v_{z0} equal the its phase velocity $v_{z0} = v_{\phi 1} = \omega\beta_1^{-1}$.

Let the system be placed in a constant and uniform magnetic field with the magnetic flux density B_0 oriented along the z axis as shown in Fig. 15.

Each electron injected parallel to the axis of a circularly polarized slow electromagnetic wave at the velocity equal to the phase velocity of this wave is equally and monotonically decelerated by its longitudinal electric field. The transverse electric field of the slow wave gives rise to the transverse velocity of the electron that, together with the longitudinal constant magnetic field (the Lorentz force), displaces it toward the region of the decelerating longitudinal electric field of the circularly polarized wave. It is important to emphasize that the degree of deceleration is independent of the time of the electron's entrance into the wave field. Therefore, the filamentary electron beam remains monoenergetic after such interaction and can be efficiently recuperated using a low-potential collector.

From the standpoint of the physics of transverse electron-beam waves (see Section 2.2), the interaction shown in Fig. 15 corresponds to the active coupling of a circularly polarized traveling electromagnetic wave and a right-polarized synchronous wave of the electron beam (R_{2+}) having negative kinetic power [see expression (25)].

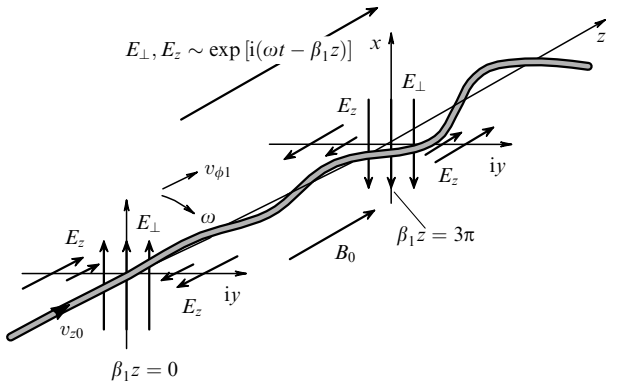

Figure 15. Diagrammatic illustration of the principle of action of a circularly polarized traveling wave tube.

Circular polarization of the electric field of an interacting wave is usually achieved by twisting the SWS. If the slow-wave system in the form of a two-row comb with π-mode oscillations [6, 53] has the fundamental wave propagation constant β, then the spatial twist of this SWS with a pitch Λ_t much greater than the comb pitch results in the splitting of circular right- and left-polarized wave propagation constants into $\beta_1 = \beta + \beta_t$ and $\beta_2 = \beta - \beta_t$, where $\beta_t = 2\pi/\Lambda_t$. Synchronism is realized only with one of these waves: $v_{z0} = v_{\phi 1} = \omega(\beta + \beta_t)^{-1}$. It has been calculated that given the appropriate choice of β_t/β, the influence of the second circularly polarized field component may be neglected [30, 55]. Other types of spatially twisted SWSs, besides the comb, may prove equally promising, e.g., a round waveguide with a two-track helical slot [58].

The amplification process in a circularly polarized traveling wave tube is usually limited by two main mechanisms: (1) violation of the synchronism condition $v_{z0} = v_{\phi 1} = \omega(\beta + \beta_t)^{-1}$ due to the beam deceleration during transmission of its energy to the wave and (2) distortion of the cross section of a real electron beam of finite diameter.

In the linear amplification region, the cross section of an electron beam retains its round shape whereas the beam itself is shifted to the maximum of the decelerating electric field of the circularly polarized wave. In the nonlinear region, the electron beam cross section loses its original shape and part of the electrons drift from the deceleration to the acceleration phase [22, 30, 59].

By way of example, Fig. 16a presents the results of numerical simulation and optimization of one of the variants of the CPTWT [60, 61], with the input power ~ 160 kW. Helix-type discretization of the electron beam was used to construct the model (see Section 2.5). Electron efficiency (η_e) of the order of 40% proved sufficient to readily ensure an 80% efficiency with recuperation using a single-stage collector in the operating frequency band $\Delta\lambda$ some 30% of the average working wavelength band λ_0. The calculations were

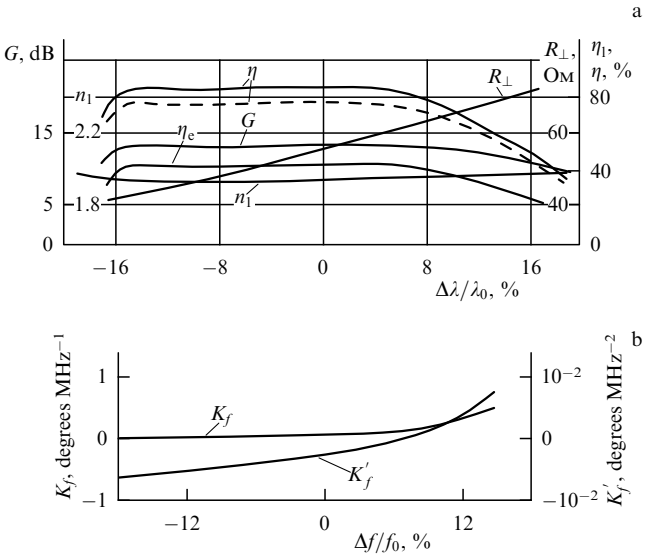

Figure 16. Results of simulation of a powerful CPTWT. G — amplification coefficient, η_e — electron efficiency, η — efficiency with recuperation of energy by a single-stage collector, $n_1 = c/v_{\phi 1}$ — deceleration coefficient of phase velocity of the circularly polarized wave, $R_\perp$ — resistance to the coupling with the DS transverse electric field, K_f and K'_f — nonlinearity coefficients of the phase – frequency characteristic of the CPTWT.

carried out at the following values of the main parameters: initial electron beam radius 1 mm, electron beam current 4.3 A, beam voltage 94 kV, magnetic flux density of the external magnetic field 0.15 T, $\lambda_0 = 11$ cm; parameters of the SWS in the form of a twisted two-row comb: radius of the interaction channel 5.5 mm, height of the comb tooth 13.5 mm, tooth width 10 mm, tooth thickness 10.3 mm, intertooth interval 4.7 mm, spatial rotation period 335 mm, length of the interaction region (comb length) 955 mm. Resistance to coupling with the comb transverse field is

$$R_\perp = \frac{|E_\perp|^2_{x=y=0}}{2\beta_1^2 P_\Sigma}\,, \tag{72}$$

where P_Σ is the power of the electromagnetic wave propagating along the comb; computation in the absence of an electron beam indicates that it varies from 20 to 70 Ωm in the operating frequency band (Fig. 16a). The value of η (the dashed curve in Fig. 16a) may be somewhat decreased in the presence of the circularly polarized component of the wave field due to the excitation of additional velocity dispersion. We emphasize that the values of η are given for a one-stage collector. The result can be improved by the use of a two-stage collector.

Phase increment in an amplifier, $\Delta\Phi$, can be written as the sum of two terms containing linear and nonlinear dependences on the operating frequency f,

$$\Delta\Phi = Af + \Phi_{\text{nonl}}(f)\,, \tag{73}$$

where A is a constant.

Of interest are usually the first and the second derivatives

$$K_f = \frac{\mathrm{d}}{\mathrm{d}f}\Phi_{\text{nonl}}(f)\,, \quad K_f' = \frac{\mathrm{d}^2}{\mathrm{d}f^2}\Phi_{\text{nonl}}(f)\,, \tag{74}$$

whose values are given in the operating frequency band in Fig. 16b. The values of K_f calculated in the maximally efficient regime do not exceed 0.55 degrees MHz^{-1} and K_f' is not higher than 8×10^{-3} degrees MHz^{-2}, i.e., much better than the respective parameters of a TWT with longitudinal grouping of the electron beam. This improvement is a direct result of a different (transverse) type of electron beam spatial grouping that is not accompanied by the formation of electron bunches (see Fig. 2).

An experimental variant of the CPTWT [62, 63] was tested at the continuous output power around 2 kW (Fig. 17). The results of the experiment were subsequently explained [64] based on the interactions in this device calculated from a model with a helix-type discretization of the injected electron beam (see Section 2.5).

In conclusion, it is noteworthy that double-cascade CPTWTs with an enhanced amplification coefficient and a reduced risk of self-excitation are also feasible and equally efficient [65].

Figure 17. Experimental variant of a CPTWT (a) and fragments of the slow-wave system in the form of a spatially twisted two-row comb (b).

8. Cyclotron-wave converter (CWC)

Current trends in the application of microwave beams for the development of energy transportation systems [15–18, 66, 67] pose a new problem — the creation of powerful devices for high-efficiency back conversion of microwave energy into the energy of direct current. The so-called rectennas (rectifying antennas) constructed from Schottky barrier diodes and half-wave dipoles demonstrate the possibility, in principle, to construct highly efficient systems for power transmission by microwaves [16–18, 66, 67]. However, rectennas are small-power low-voltage devices subject to failures.

A converter [68–73] essentially devoid of these drawbacks is represented in Fig. 18. In its input resonator, practically all microwave power from an external source is introduced into a FCW of the electron beam. It makes the beam rotate about the z axis at the angular frequency $\omega = \omega_c$. In the next section of the device, magnetic flux density of the static reverse magnetic field changes from B_0 to $B_1 < 0$. This section harbors the radial component B_r of the magnetic flux density [see Eqn (43)], and the energy of electron beam rotation is converted into the additional energy of its longitudinal motion. This additional energy is then released during recuperation at the outside load of the collector whose potential is below the cathode potential.

In terms of physical processes proceeding in the input resonator of the cyclotron energy converter, it is no different from the resonators used in CWPs, CWPAs or CWESAs, barring the larger size of its interaction region. The real efficiency of microwave energy conversion into the energy of electron beam rotation is estimated at 0.95–0.98.

The processes in the reversed region were simulated by means of helix-type discretization of the electron beam (see Section 2.5). The results of simulation indicate that the maximum efficiency of conversion of the electron beam rotation energy into the energy of longitudinal motion is usually realized in the case of asymmetric distribution of the magnetic field in the reversed region ($B_0 > |B_1|$); it also depends on the length of this region ($z_2 - z_1$ in Fig. 18), the electron beam radius, and the radius of beam rotation around the z axis at the inlet of this region. An efficiency of energy conversion of the order of 85–95% is not unlikely in such devices given optimized parameter values [68–73]. The internal Coulomb fields of the electron beam are of minor importance as long as the current remains within 0.75–0.85 of the Brillouin value [30, 70, 72, 73].

In the reverse region, the energy of an electron beam FCW is converted to FSW energy.

The overall efficiency of the device depends on both the collector and the collector region. Secondary emission from the surface of the collector presents a real danger because the collector potential is lower than the potential of the cathode and the resonator. However, an additional electrode with an even lower potential placed in front of the collector creates the potential distribution that substantially prevents the outflow of secondary electrodes from the collector [71].

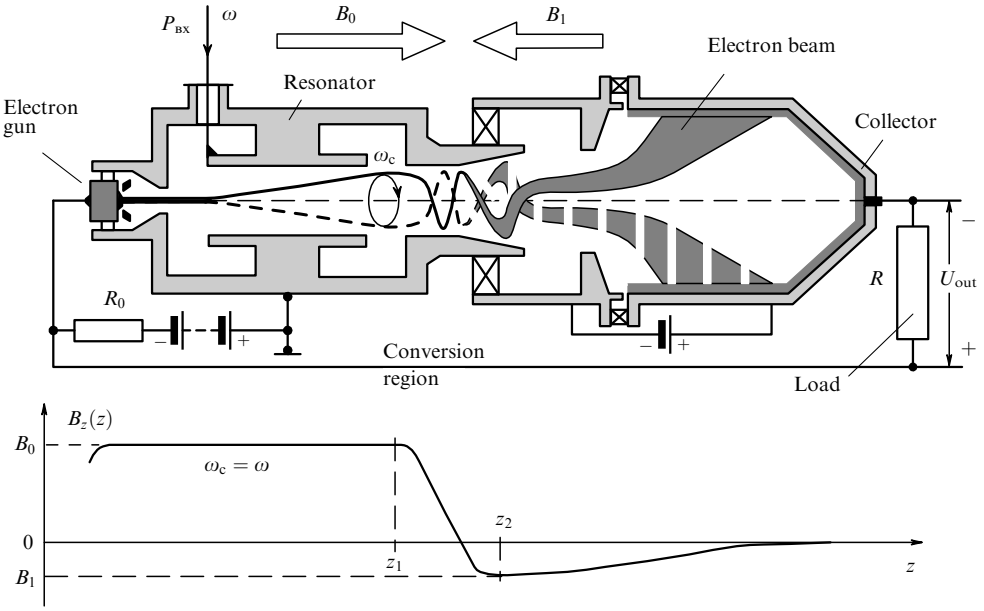

Figure 18. Schematic representation of a cyclotron wave converter.

In the case of high overloads by input signals, the electron beam begins to be partly intercepted by the input resonator bars while high ohmic resistance R_0 (Fig. 18) causes a sharp decrease in the resonator potential with respect to the cathode potential; as a consequence, the electron beam is halted (or considerably restricted). When the input power falls below a relatively optimal level, the reflection of the electron beam starts in the collector region and leads to the same outcome due to the appearance of the current at the outer casing of the device.

High efficiency values at large power and output voltage levels, freedom from operational failures, good reliability, and the absence of problems associated with excessive emission of harmonics are the main attractive features of CWCs (as opposed to rectennas).

Experimental variants of the CWC were tested at Lomonosov Moscow State University, Istok and Tory State Research and Production Corporations at the frequency 2.45 GHz and power levels varying from several dozen watts to 10 kW, with the efficiency between 70 and 83%. Some of these models are presented in Fig. 19.

The cyclotron resonance condition $\omega = \omega_c$ requires relatively high values of the magnetic flux density, especially in the shortwave segment of the centimeter wavelength region and in the millimeter region. This problem can be partially obviated [74–76] by transforming the external signal energy into FCW energy in a quadrupole resonator like that shown in Fig. 8. In this case, the cyclotron resonance condition has the form $\omega_c = \omega/2$. This means that the magnetic system of such a CWC must ensure the cyclotron frequency twice as low as the operating frequency. However, the quadrupole resonator has no electric field on its axis. Hence, the necessity of a minor preliminary modulation of the flow on the FCW is achieved with the aid of a uniform field resonator working at the frequency $\omega/2$ and fed from the same source. The supply circuit of this resonator is simple and may be placed inside the device; it includes a coupler taking a small part of the total power (less than 1%) aside, a frequency divider, and a phase shifter.

Accordingly, an octupole resonator allows the resonant magnetic field to be decreased three times.

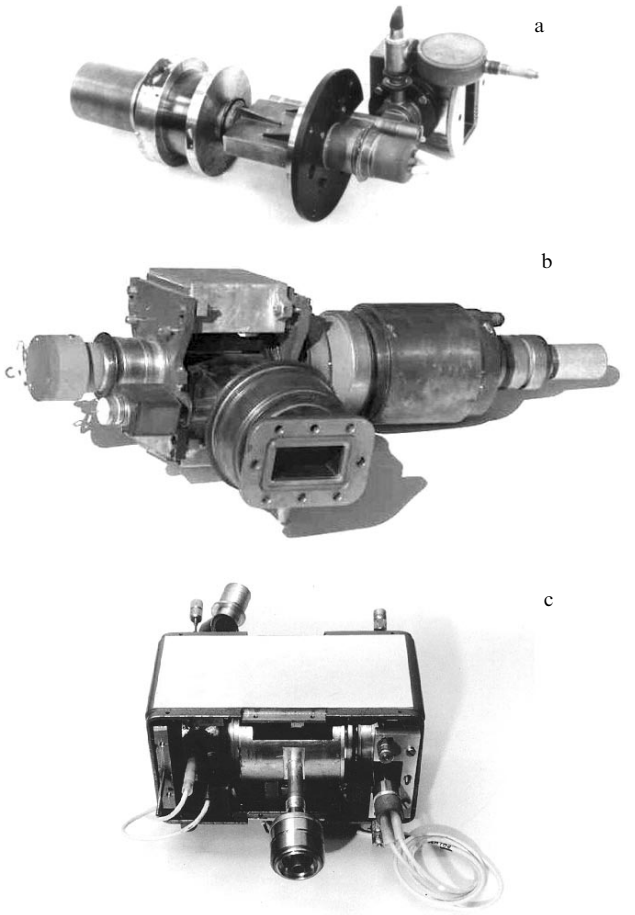

Figure 19. Experimental variants of cyclotron wave converters for power levels of (a) 10 kW in the pulsed regime (magnetic system is not shown), (b) 10 kW in the continuous regime, and (c) 300–500 W in the continuous regime [34, 72, 73].

9. The klystron with combined interaction (KCI)

We now briefly discuss the possibility of using combined longitudinal–transverse interaction for the extension of the operating frequency band of the transit-time klystron [77]. Multicavity groupers of modern klystrons make it possible to form compact electron bunches. These bunches are injected into a reversed magnetic field region with a certain shift Δ with respect to the field axis as shown in Fig. 20. The magnetic flux density at the outlet of the reversed region corresponds to the cyclotron resonance, $\omega_c = \omega$.

Each electron bunch passing through the reversed region loses part of its longitudinal motion energy and starts to rotate at the frequency $\omega_c = \omega$.

The bunches appear at the outlet of the grouper with the intervals $T = 2\pi/\omega$; therefore, when leaving the reversed region, they occur on one straight line rotating as a whole around the z axis. The energy of electron beam rotation can be extracted from the beam in a transverse electric field resonator (see Fig. 20). It is worth noting that the very existence of electron bunches and their subsequent longitudinal dispersion in the uniform transverse electric field of the output resonator is no longer essential. The appropriate choice of the shift Δ ensures the conditions under which a major part of the energy of electron beam longitudinal motion is converted into the energy of beam rotation. This energy is then almost completely extracted in the output resonator.

For a transverse field resonator (see Fig. 20), the active parallel transmission introduced by the electron beam is

$$G_{\text{trans}} = \frac{1}{8}\,\frac{I_0}{U_0}\left(\frac{l}{d}\right)^2, \tag{75}$$

where I_0, U_0 are the electron beam current and potential and l, d are the bar length and the gap between them, respectively.

For the output longitudinal field resonator of a klystron, in the interaction region,

$$G_{\text{long}} \approx \frac{2I_0}{(1.3-1.5)\,U_0}. \tag{76}$$

Usually, $l^2/d^2 \approx 50-100$, and hence $G_{\text{trans}}/G_{\text{long}} \approx 10-15$. Assuming the characteristic resistances of these two types of resonators to be roughly identical, it can be estimated that the operating band of the output resonator of the klystron may be extended approximately 10–15 times. Joule losses in this resonator will be decreased as much.

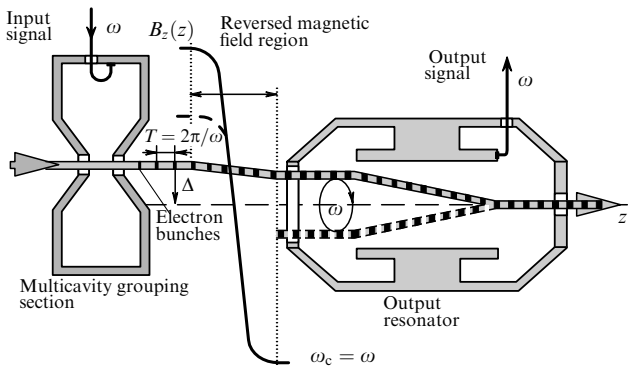

Figure 20. Schematic diagram of a klystron with combined longitudinal–transverse interaction.

10. Discussion

A relatively simple idea underlies the principles of amplification and generation of microwave-range electromagnetic oscillations by an electron beam. It consists of the placement of electrons of this beam largely in decelerating half-periods of the external microwave electromagnetic field. In this case, the electrons are on the whole decelerated, delivering part of their motion energy to the external magnetic field.

When the external electric field is directed parallel to the electron beam (see the top part of Fig. 2), the accelerating and decelerating half-periods of this field occupy discrete areas along the flow (resonator gap fields or half-periods of the traveling wave field), thus making the formation of electron bunches inevitable. Denser bunches ensure more efficient energy transmission from the electron beam to the external field. On the other hand, bunching (especially formation of denser bunches) suggests the appearance of strong and spatially nonuniform Coulomb fields showing a nonlinear dependence on many factors, including the signal level. These fields tend to destroy bunches by interfering with their formation and energy exchange with the external field and also by introducing additional nonlinearity into these processes.

The picture remains basically the same when the interaction occurs in the so-called crossed fields (magnetron, TWT-M, etc.); however, electron bunching is equally indispensable in this situation.

In the second case (see Fig. 2, bottom), the external uniform electric field is directed across the electron beam drifting in the external stationary magnetic field. The external linearly polarized field can be represented as the sum of two circularly polarized components. Only one of them is involved in adiabatically accumulating interaction, in agreement with the selected direction of the magnetic field B_0. Decelerating and accelerating half-periods for circularly polarized waves are continuously distributed in space. The electron beam interacting with these waves is spatially twisted but contains no bunches (Figs 3b, 4, 6, 15), and the beam geometry is usually such that it is possible to neglect the Coulomb fields associated with this twisting.

Thus:

1. Excitation of transverse (cyclotron and synchronous) waves, unlike that of spatial charge waves, is unrelated to the compression of the spatial charge inside the electron beam. This permits avoiding nonlinearities induced by the internal and external Coulomb fields of electron bunches. The relativistic (nonlinear) dependence of the electron mass on its energy is inapplicable here.

2. Circular polarization of transverse electron-beam waves together with the stability and predictability of their phase velocities ensures a high degree of selectivity of energy exchange between cyclotron/synchronous waves and external electromagnetic fields.

3. It is relatively easy to realize regimes in which kinetic powers of transverse waves are comparable with or larger than the power of longitudinal beam motion.

These three physically simple factors permit obviating many difficulties that substantially slow further progress in vacuum microwave electronics based on the principles of longitudinal grouping of electron beams.

Transverse electron-beam waves may be used in a large variety of devices for vacuum microwave electronics including protectors, parametric and electrostatic amplifiers, circularly

polarized traveling wave tubes, converters of microwave energy to direct current, etc. The application of these devices appears very promising in such fields as scientific research (radioastronomy, EPR, NMR, charged-particle accelerators, etc.), communications and informatics, radiolocation, radionavigation, and cosmic energetics [15 – 18].

Input devices (CWPs, CWPAs, CWESAs) possess a rare combination of high sensitivity and broad dynamic range; in addition, they are capable of sustaining high overloads by input signals and ensure reliable protection of subsequent receiver cascades, the absence of leakage power peaks, and the substantial reduction of time needed for the restoration of serviceability after overloads.

During the broadband interaction of an electron beam with a circularly polarized traveling wave (as in CPTWTs), large output power levels combine with high efficiency and unique linearity of phase frequency characteristics of nonlinear regimes.

Devices in which the microwave energy is converted back into the energy of direct current (CWCs) operate at large power levels with high efficiency and input voltage; also, they are resistant to the overloading of their low-frequency and high-frequency circuits.

In specific cases, combined longitudinal – transverse interactions may be effectively employed, for example, to extend the operating frequency band and reduce joule losses in the output resonator of a KCI.

The present paper does not pretend to highlight the entire spectrum of problems related to transverse electron-beam waves. It only briefly touches on those considered high priority items by the author [78, 79].

Suffice it to mention powerful cyclotron phase shifters [80], amplifiers of cyclotron-synchronous waves [51, 52], and principles of reducing cyclotron wave noises with the aid of lossless noise transformers [81].

In the last few years, the Istok State Research and Production Corporation has manufactured and sold over 10,000 various devices based on the use of cyclotron electron-beam waves.

The currently available results of theoretical and experimental studies briefly discussed in this review give reason to speak about the feasibility and good prospects of further extension of the spectrum of microwave electronic devices based on the use of transverse (cyclotron and synchronous) electron-beam waves and possessing unique combinations of working parameters.

The author considers it his pleasant duty to remember, with feelings of great respect and gratitude, Samson Davidovich Gvozdover, Vladimir Mikhailovich Lopukhin, and Sergei Pavlovich Kantyuk, who initiated and headed the works on transverse electron beam waves for microwave electronics in this country.

The author is grateful to Yu A Budzinskii and S V Bykovskii for their help and many enlightening discussions of different parts of this publication.

Last but not the least, the author wishes to dedicate this paper to the fond memory of his deceased wife, whose many years' support and assistance made the majority of his studies cited here possible.

References

1. Lopukhin V M *Vozbuzhdenie Elektromagnitnykh Kolebanii i Voln Elektronnymi Potokami* (Excitation of Electromagnetic Oscillations and Waves by Electron Beams) (Moscow: Gostekhizdat, 1953)
2. Kalinin V I, Gershtein V M *Vvedenie v Radiofiziku* (Introduction to Radiophysics) (Moscow: Gostekhizdat, 1957)
3. Pierce J R *Travelling-Wave Tubes* (New York: Van Nostrand, 1950) [Translated into Russian (Moscow: Sov. Radio, 1952)]
4. Gvozdover S D *Teoriya Elektronnykh Priborov Sverkhvysokikh Chastot* (Theory of Microwave Electron Devices) (Moscow: Gostekhizdat, 1956)
5. Shevchik V N, Shvedov G N, Soboleva A V *Volnovye i Kolebatel'nye Yavleniya v Elektronnykh Potokakh na Sverkhvysokikh Chastotakh* (Wave and Oscillation Phenomena in Electron Flows at Ultrahigh Frequencies) (Saratov: Izd. Saratovskogo Univ., 1962)
6. Al'tshuler Yu G, Tatarenko A S *Lampy Maloi Moshchnosti s Obratnoi Volnoi* (Low-Power Backward Wave Tubes) (Moscow: Sov. Radio, 1963)
7. Fedorov M M (Ed.) *Elektronnye Sverkhvysokochastotnye Pribory so Skreshchennymi Polyami* Vol. 1, 2 (Ultrahigh-Frequency Crossed-Field Devices (Moscow: IL, 1961)
8. Kapitsa P L *Elektronika Bol'shikh Moshchnostei* (High-Power Electronics) (Mocsow: Izd. AN SSSR, 1962)
9. Stal'makhov V S *Osnovy Elektroniki Sverkhvysokochastotnykh Priborov so Skreshchennymi Polyami* (Fundamentals of Electronics of Ultrahigh-Frequency Crossed-Field Devices) (Moscow: Sov. Radio, 1963)
10. Gaponov A V, Petelin M I, Yulpatov V K *Izv. Vyssh. Ucheb. Zaved., Ser. Radiofiz.* **10** 1414 (1967)
11. Roy J E *The Theory of Non-Linear Phenomena in Ultrahigh-Frequency Devices* [Translated into Russian (Moscow: Sov. Radio, 1969)]
12. Shevchik V N, Trubetskov D I *Analiticheskie Metody Rascheta v Elektronike SVCh* (Analytical Computation Methods in Electronics) (Moscow: Sov. Radio, 1970)
13. Vainshtein L A, Solntsev V A *Lektsii po Sverkhvysokochastotnoi Elektronike* (Lectures on Ultrahigh-Frequency Electronics) (Moscow: Sov. Radio, 1973)
14. Gulyaev Yu V, Kravchenko V F, Kuraev A A *Usp. Fiz. Nauk* **174** 639 (2004) [*Phys. Usp.* **47** 583 (2004)]
15. Glaser P E *Science* **162** 857 (1968)
16. Vanke V A, Lopukhin V M, Savvin V L *Usp. Fiz. Nauk* **123** 633 (1977) [*Sov. Phys. Usp.* **20** 989 (1977)]
17. Vanke V A, Leskov L V, Luk'yanov A V *Kosmicheskie Energosistemy* (Space Energy Systems) (Moscow: Mashinostroenie, 1990)
18. Nagatomo M, Sasaki S, Nuruo Y *Usp. Fiz. Nauk* **164** 631 (1994) [*Phys. Usp.* **37** 589 (1994)]
19. Lopukhin V M, Roshal' A S *Usp. Fiz. Nauk* **85** 297 (1965) [*Sov. Phys. Usp.* **8** 117 (1965)]
20. Vanke V A, Lonukhin V M, Savvin V L *Usp. Fiz. Nauk* **99** 545 (1969) [*Sov. Phys. Usp.* **12** 743 (1970)]
21. Bogolyubov N N, Mitropol'skii Yu A *Asimptoticheskie Metody v Teorii Nelineinykh Kolebanii* (Asymptotic Methods in the Theory of Non-Linear Oscillations) (Moscow: Fizmatgiz, 1963) [Translated into English (New York: Gordon and Breach Sci. Publ., 1961)]
22. Vanke V A, D.Sc. Thesis (Moscow: Moscow State Univ., 1981)
23. Vanke V A *J. Radioelectron.* (1) (2002); http://jre.cplire.ru/jre/jan02/2/text_e.html
24. Louisell W H *Coupled Mode and Parametric Electronics* (New York: Wiley, 1960) [Translated into Russian (Moscow: IL, 1963)]
25. Dubravec V *Arch. Elektr. Übertrag.* **18** 585 (1964)
26. Lopukhin V M et al. *Shumy i Parametricheskie Yavleniya v Elektronnykh Priborakh Sverkhvysokikh Chastot* (Noises and Parametric Phenomena in Ultrahigh-Frequency Electronic Devices) (Moscow: Nauka, 1966)
27. Lopukhin V M, Roshal' A S *Elektronnoluchevye Parametricheskie Usiliteli* (Electron Beam Parametric Amplifiers) (Moscow: Sov. Radio, 1968)
28. Dubravec V *Electron. Commun.* **39** 558 (1964)
29. Adler R, Ashkin A, Gordon E I *J. Appl. Phys.* **32** 672 (1961)
30. Zaitsev A A, Ph.D. Thesis (Moscow: Moscow State Univ., 1979)
31. Smith L P, Shulman C I *Proc. IRE* **35** 644 (1947)
32. Cuccia C L *RCA Rev.* **10** 270 (1949)
33. Cuccia C L *RCA Rev.* **21** 228 (1960)
34. Budzinski Yu A et al. *Radiotekhnika* **32** (4) 18 (1999)
35. Bykovskii S V, Ph.D. Thesis (Moscow: GNPP 'Istok', 1997)

36. Boudzinski Yu A, Kantyuk S P *Proc. IEEE MTT-S Digest* **2** 1123 (1993)
37. Boudzinski Yu A, Bykovski S V, in *Proc. 2nd IEEE Intern. Vacuum Electron. Conf., April 2–4, 2001, Noordwijk, The Netherlands*, p. 321
38. Adler R *Proc. IRE* **46** 1300 (1958)
39. Adler R, Hrbek G, Wade G *Proc. IRE* **46** 1756 (1958)
40. Vanke V A, Grigorenko L P, Magalinskii V B *Radiotekh. Elektron.* **10** 2187 (1965)
41. Vanke V A, Lopukhin V M, Kantyuk S P *Radiotekh. Elektron.* **14** 666 (1969)
42. Vanke V A, Magalinskii V B *Izv. Vyssh. Ucheb. Zaved., Ser. Radiofiz.* **9** 831 (1966)
43. Hrbek G, Adler R, in *Proc. 5th Intern. Congress Microwave Tubes* (New York: Academic Press, 1965) p. 17
44. Vanke V A, Matsumoto H, Shinohara N *IEICE Trans. Electron.* (Japan) **E81-C** 788 (1998)
45. Vanke V A, Matsumoto H, Shinohara N J. Radioelectron. (10) (1999); http://jre.cplire.ru/jre/oct99/1/text.html
46. Adler R, Wade G *J. Appl. Phys.* **31** 1201 (1960)
47. Vanke V A, Savvin V L *Radiotekh. Elektron.* **15** 2317 (1970)
48. Vanke V A, Kryukov S P *Radiotekh. Elektron.* **17** 2230 (1972)
49. Vanke V A, Kryukov S P *Izv. Vyssh. Uchebn. Zaved. Ser. Radiofiz.* **16** 1271 (1973)
50. Bass J S *Proc. IRE* **49** 1424 (1961)
51. Vanke V A, Timofeev Yu *Izv. Vyssh. Uchebn. Zaved., Ser. Radiofiz.* **15** 615 (1972)
52. Vanke V A, Timofeev Yu *Izv. Vyssh. Uchebn. Zaveb., Ser. Radiofiz.* **16** 1751 (1973)
53. Silin R A, Sazonov V P *Zamedlyayushchie Sistemy* (Slow-Wave Structures) (Moscow: Sov. Radio, 1966)
54. Vanke V A et al. *Izv. Vyssh. Uchebn. Zaved., Ser. Radiofiz.* **15** 291 (1972)
55. Vanke V A, Zaitsev A A, Moshkov A V *Izv. Vyssh. Uchebn. Zaved., Ser. Radiofiz.* **21** 590 (1978)
56. Vanke V A, Konnov A V *Radiotekh. Elektron.* **31** 572 (1986)
57. Vanke V A, Konnov A V *Radiotekh. Elektron.* **33** 1544 (1988)
58. Vanke V A, Konnov A V *Radiotekh. Elektron.* **32** 1994 (1987)
59. Vanke V A, Konnov A V, Savvin V L *Radiotekh. Elektron.* **34** 2577 (1989)
60. Vanke V A, Konnov A V, Savvin V L *Elektron. Tekh., Ser. Elektron. SVCh* (4 (398)) 20 (1987)
61. Vanke V A, Konnov A V, Savvin V L *Radiotekhn. Elektron.* **34** 1517 (1989)
62. Nigmatullin U A, Ph.D. Theses (Moscow: Moscow State Univ., 1978)
63. Yur'ev V I et al. *Radiotekh. Elektron.* **17** 830 (1972)
64. Vanke V A, Zaitsev A A, Nigmatullin U A *Radiotekh. Elektron.* **26** 2365 (1981)
65. Vanke V A, Konnov A V, Savvin V L *Radiotekh. Elektron.* **35** 1549 (1990)
66. Brown WC *IEEE Trans. Microwave Theory Techn.* **MTT-32** 1230 (1984)
67. Brown W C, in *Proc. 3rd Intern. Conf. Wireless Power Transmission, August 24–28, 1997 Montreal*, p. 177
68. Bardenkov V A et al. *Radiotekh. Elektron.* **21** 821 (1976)
69. Bykovskii S V et al., Patent RF (RF Patent) No 2119691 (1998)
70. Vanke V A *Radiotekh. Elektron.* **23** 1217 (1978)
71. Bleivas I M et al. *Radiotekh. Elektron.* **27** 1009 (1982)
72. Vanke V A et al. *IEICE Trans. Electron.* (Japan) **E81-C** 1136 (1998)
73. Vanke V A et al. *J. Radioelectron.* (9) (1999); http://jre.cplire.ru/jre/sep99/1/text.html
74. Matsumoto H, Vanke V A, Shinohara N, US Patent No. 6, 507, 152 B2 (2003)
75. Vanke V A *J. Radioelectron.* (4) (2002); http://jre.cplire.ru/jre/apr02/6/text.html
76. Vanke V A, Matsumoto H, Shinohara N *IEICE Trans. Electron.* (Japan) **E-86-C** 1390 (2003)
77. Vanke V A, Gorelikov V I, Savvin V L, Avt. svid. (Certificate of Invention) No 1086986 (1983)
78. Vanke V A et al. *J. Radioelectron.* (3) (2002); http://jre.cplire.ru/jre/mar02/5/text_e.html
79. Vanke V A, in *Proc. 3rd IEEE Intern. Vacuum Electron. Conf., April 23–25, 2002, Monterey, California, USA*, p. 196
80. Vanke V A et al., Author's Certificate No 3781234 (1984)
81. Vanke V A, Kryukov S P, Timofeev Yu M *Izv. Vyssh. Uchebn. Zaved., Ser. Radiofiz.* **14** 142 (1971)